

DESIGN AND CONSTRUCTION
of a
HIGH-DISPERSION INFRA-RED SPECTROGRAPH

by

GEORGE ALBERT BREALEY

A THESIS SUBMITTED IN PARTIAL FULFILMENT OF
THE REQUIREMENTS FOR THE DEGREE OF
MASTER OF APPLIED SCIENCE
in the Department
of
PHYSICS

We accept this thesis as conforming to the
standard required from candidates for the
degree of MASTER OF APPLIED SCIENCE.

Members of the Department of

THE UNIVERSITY OF BRITISH COLUMBIA

April, 1951

ABSTRACT

Details are given of the design and construction of a single-beam, three-prism, infra-red spectrograph, to be used in the near infra-red region 0.7μ to 2.5μ for the purpose of examining fine structure in molecular bands in this region.

The problems encountered and methods of solution are explained. Details are presented of the optical and mechanical design of the instrument. The radiant energy transmitted by the spectrograph falls on a PbS photoconducting cell after being chopped at 900 c.p.s. The resulting signal is amplified in a tuned amplifier and, after rectification, is recorded on a Brown recording potentiometer. Details of detector and amplifier are presented.

The method of calibration is explained and the performance of the instrument in practice is assessed by consideration of typical spectra taken with the final assembly.

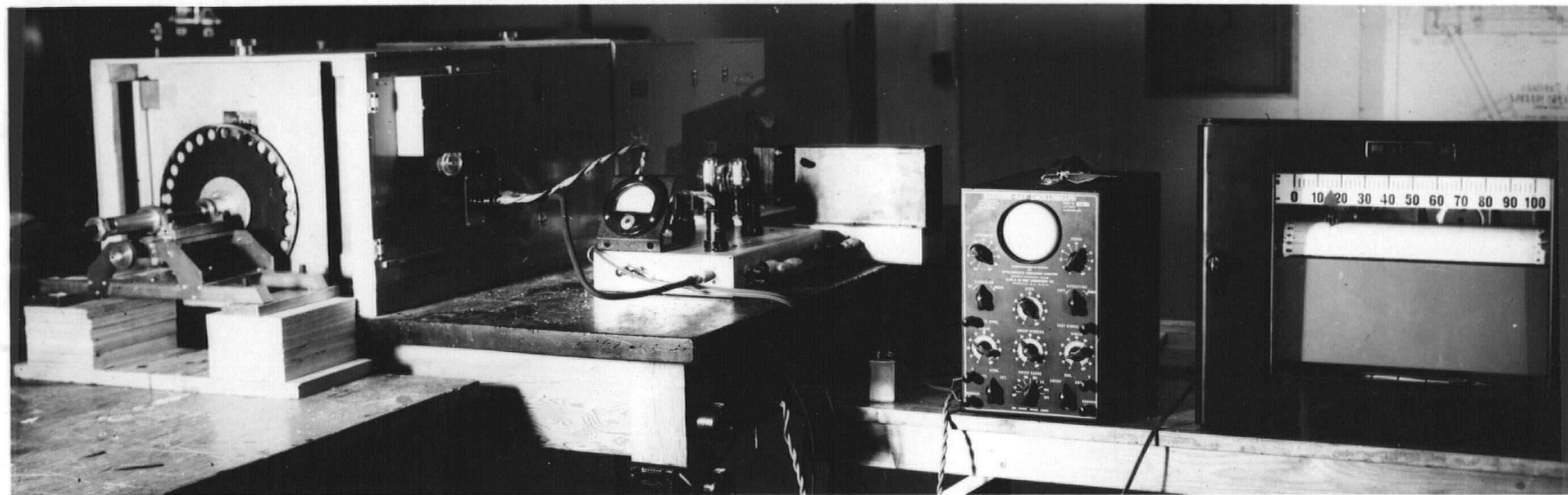
FRONTISPIECE

TWO VIEWS OF THE SPECTROGRAPH

The complete instrument

and

The optical portion



ACKNOWLEDGEMENTS

The author wishes to express his indebtedness to the following persons, without whose help and advice the task undertaken would have presented nearly insurmountable difficulties:

Dr. A. M. Crooker, under whose supervision this project was carried out.

Messrs. Fraser and Meier, for invaluable assistance with milling and fine-machining operations.

Messrs. Price and Tomlinson, for considerable advice in electronics.

The Scholarship Committee of the Department of Veterans' Affairs, for extending the author's rehabilitation grants for the two years required to complete this project.

The British Columbia Telephone Company for financial assistance in the form of a scholarship for the last year of the work.

The University of British Columbia

April 20, 1951

George Albert Brealey

CONTENTS

	Page No.
Acknowledgements	i
Introduction	ii
List of Plates	vi
List of Figures	vii
List of Tables	viii
CHAPTER 1 The Spectrograph: Prism Theory and Optical and Electronic Sequences	1
A. The Theory of the Prism Spectrometer	
B. The Proposed Spectrograph	
CHAPTER 2 Calculations Applying to the Geometric Optics of the Light Path	7
A. The Prisms	
B. The Lens	
CHAPTER 3 The Prism Table and Scanning Drive	25
A. Introduction	
B. Rotation of the Prism Table	
C. The Scanning Drive	
CHAPTER 4 The Mirror and the Slits	31
A. The Off-Axis Paraboloid	
B. The Exit Slit Mirror	
C. The Slit Mechanism	
D. The Slit Jaws	
CHAPTER 5 Electronic Components	37
A. Introduction	
B. The Photoelectric Cell	
C. The Chopping Wheel and Motor	
D. Choice of Amplifier: The Pre-Amplifier	
E. The Main Amplifier and Power Supply	
F. The Performance of the Amplifier	

CONTENTS - continued

	Page No.
CHAPTER 6 Final Assembly	48
A. Introduction	
B. Optics	
C. Enclosing the Spectrograph	
D. Electronic Components	
CHAPTER 7 Results of Spectra taken with the Spectrograph: Conclusions	52
A. Introduction	
B. Experimental	
C. Conclusions	
Bibliography	ix
Reproductions of Working Drawings for Spectrograph	Appendix A
1. Assembly of the Infra-Red Spectrograph	
2. Drive for Prism Table	
3. Assemblies of Prism Table and Mirror Cell	
4. Slit Assembly and Base Mount	
5. Prism Table Detail. Drive Base Plate. Motor Mount	
6. Detail of Slits	
7. Detail of Drive Linkage	
8. Spectrograph Mountings; Gratings and Mirror	

LIST OF PLATES

Plate No.		Following Page No.
I	The Prism Table and Mirror Assemblies . .	26
II	The Driving Mechanism	28
III	The Pre-Amplifier, Photocell, and Slits	32
IV	Front View of Optical Assembly	48
V	Rear View of Optical Assembly	49
VI	The Complete Spectrograph	50
VEI	Spectrum of Hg I taken with the Spectrograph	52

LIST OF FIGURES

Chapter No.	Figure No.		Page No.
1	1.1	Block diagram of sequences in the spectrograph	3
	1.2	Optical sequence (lens collimation)	4
	1.3	Optical sequence (mirror collimation)	5
2	2.4	Finding N_{λ} for a half-prism	8
	2.4a	Graph of Index N of unknown glass against λ	10
	2.5	Explanation of symbols in an achromatic doublet	12
	2.6	Showing the significance of bfl and efl in paraxial ray tracing	14
	2.7	Construction for proving the Abbé invariant	15
	2.8	Axial ray trace parameters	18
	2.9	Variation of bfl, efl, and L' with λ	22
3	3.10	Prism Table	26
4	4.11	Typical Slit	33
	4.12	Exit slit jaws: construction	35
5	5.13	Pre-amplifier	41
	5.14	Main Amplifier	43
	5.15	Rectifier circuit for input to Brown Recorder	44
	5.16	Power Supply	45

LIST OF TABLES

Chapter No.	Table No.		Page No.
2	2.1	Results of measurements for the full prism	9
	2.2	N and D at violet, red, and infra-red wave lengths	11
	2.3	N_{λ} for the components of the achromatic doublet	13
	2.4	Paraxial traces of BW 19/20	17
	2.5	Axial ray trace of BW 19/20	20
	2.6	Theoretical resolving power of the spectrograph for certain wave lengths	23
5	5.7	Excerpts from data sheet. Lead Sulphide Cell Type C	39
7	7.8	Mercury I. Wave numbers and transitions of lines $\nu = 5000$ to $\nu = 10,000 \text{ cm}^{-1}$	54
	7.9	Mercury I. Wave numbers and transitions of lines 0.7_{μ} to 1_{μ}	57

INTRODUCTION

The Perkin-Elmer infra-red spectrometer has a resolving power of the order of 1 in 500 over most of its range; this is insufficient to resolve the rotational fine structure in certain molecules having bands in the region 0.7μ to 2.5μ .

It was proposed to build an infra-red spectrometer with at least double this resolving power to cover the wave length range from 0.4μ to the upper limit of the glass used in the prisms. By using one 60° prism and one half-prism silvered on its back face, effectively a three-prism instrument would result with a consequent increase in resolution by a factor of 3.

Scanning of the spectrum was to be effected by rotation of the prisms so that the exit slit received the radiation at minimum deviation at that instant. Since the response of the Lead Sulphide photo-cell is greatest in the above region, it was decided to use this device as a detector. The incident radiation was to be chopped at 900 cycles per second, and the resulting signal on the cell was to be amplified by a narrow-band tuned amplifier.

Thus the following major problems were encountered:

a) How to link the prisms mechanically so that the radiation at the exit slit had passed through the prisms at or near minimum deviation, b) how to control the rate of coverage of the spectrum so that the scanning was carried out in optimum times, and c) how to construct an amplifier which would most satisfactorily respond to changes in the conductivity of the photo-

cell and have the best possible signal-to-noise ratio.

In the text to follow, the scope and solutions of these and other problems are described in detail.

CHAPTER 1

THE SPECTROGRAPH: PRISM THEORY
AND OPTICAL AND ELECTRONIC SEQUENCES

A. THE THEORY OF THE PRISM SPECTROMETER

From any standard text on optics, certain relations may be proved between parameters characteristic of the radiation and the prism.

In the position of minimum deviation for a light ray of wave length λ ,

$$n_{\lambda} = \frac{\sin \frac{A + D_{\lambda}}{2}}{\sin \frac{A}{2}} \quad 1.1$$

where n_{λ} = index of refraction at wave length λ , D_{λ} = minimum deviation angle, and A = prism angle.

Also, in the position of minimum deviation,

$$\frac{\Delta \Theta}{\Delta n} = \frac{2 \sin \frac{A}{2}}{\sqrt{1 - n^2 \sin^2 \frac{A}{2}}} \quad 1.2$$

where Θ = angle of minimum deviation. It is thus written because the formula, although derived at minimum deviation, is very nearly true over large limits of D .

If one assume the correctness of the Cauchy formula relating n and λ ,

$$n = A + \frac{B}{\lambda^2} \quad 1.3$$

then

$$\frac{dn}{d\lambda} = - \frac{2B}{\lambda^3} \quad 1.4$$

The dispersion $\frac{d\theta}{d\lambda} = \frac{dn}{d\lambda} \cdot \frac{d\theta}{dn}$ can be found from 1.2 and 1.4 by merely taking the product of the two expressions.

By using the Rayleigh criterion for resolution, that two wave lengths are just resolved when the maximum of one falls on the first diffraction minimum of the other, it is possible to show that

$$\frac{\lambda}{a} = a \frac{d\theta}{d\lambda} \quad 1.5$$

where a = effective aperture, and $\frac{d\theta}{d\lambda}$ = angular dispersion.

Also, it can be shown that the amount of resolution possible depends only on the thickness of the base of the prism and the change in index between the two wave lengths desired resolved. That is,

$$t = \frac{\lambda}{\Delta n} \quad 1.6$$

where λ = mean wave length and Δn = change in index.

It can be shown that the foregoing results for angular dispersion and resolving power are directly proportional to the number of prisms. e.g. For three prisms all alike, $\frac{d\theta}{d\lambda}$ and $\frac{\lambda}{a}$ will be three times as great as for one prism.

It might be well to point out, in brief, wherein lies the advantage of the prism over the grating in spectroscopy. Admittedly the dispersion and resolving power on a wave length scale decrease with increasing wave length for the prism instrument, whereas this is not true for the grating. However, on an energy level scale, the energy level differences are proportional to $\Delta\nu$; so that, to resolve an energy level difference, it is necessary that the resolving power increase directly with ν .

For the prism,

$$R.P. \approx \frac{C}{\lambda^3} = \frac{\lambda}{d\lambda} \quad \text{where } C \text{ is a constant.}$$

$$\therefore d\lambda_{\min} \sim \frac{\lambda^4}{C} \quad \therefore d\nu_{\min} \sim \nu \frac{d\lambda}{\lambda} = C' \lambda^2$$

i.e., as λ increases, the magnitude of the smallest resolvable $\Delta\nu$ increases.

For the grating,

$$R.P. = mN = \frac{\lambda}{d\lambda}$$

$$\therefore d\lambda_{\min} = \frac{\lambda}{C''} \quad \therefore d\nu_{\min} = \nu \frac{d\lambda}{\lambda} = C''' \lambda^{-1}$$

B. THE PROPOSED SPECTROGRAPH

A block diagram of the proposed sequence is shown in Fig. 1.1, while a more detailed pictorial drawing of the opti-

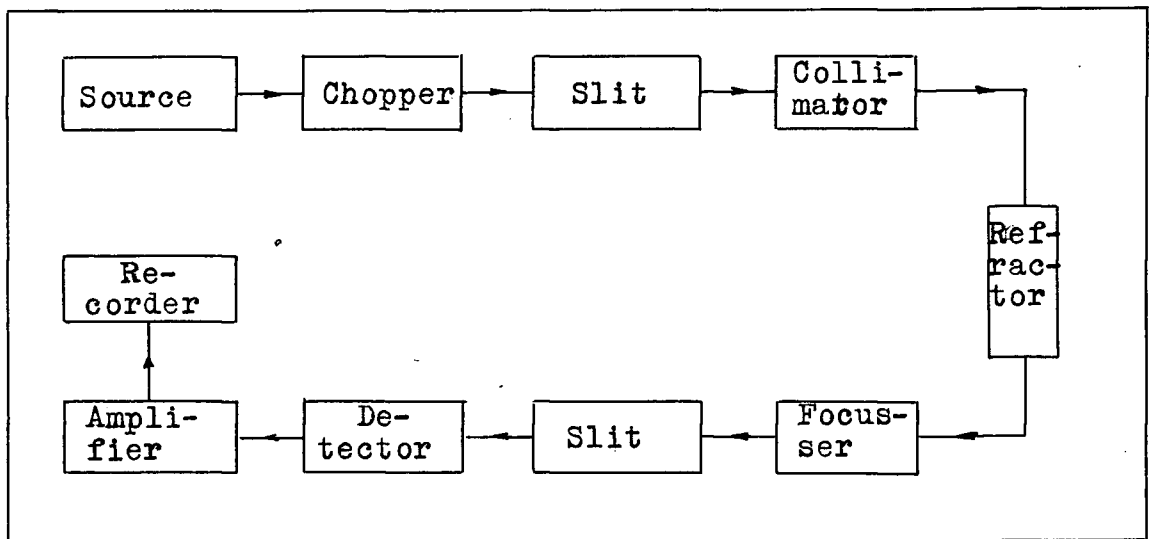


Fig.1.1. Block diagram of sequences in the spectrograph.

cal sequence is shown in Fig. 1.2. In the original design, the light from the source was to be chopped at 900 c.p.s. by the

chopping wheel C before passing through the entrance slit S. The chopped radiation was to be collimated by the lens, L, pass through the first prism, P_1 , at minimum deviation and be reflected from the back of the second prism, P_2 . After again passing through P_1 , it was to be again focussed by the lens, and be passed through the exit slit, E, by means of reflection from the small mirror, M.

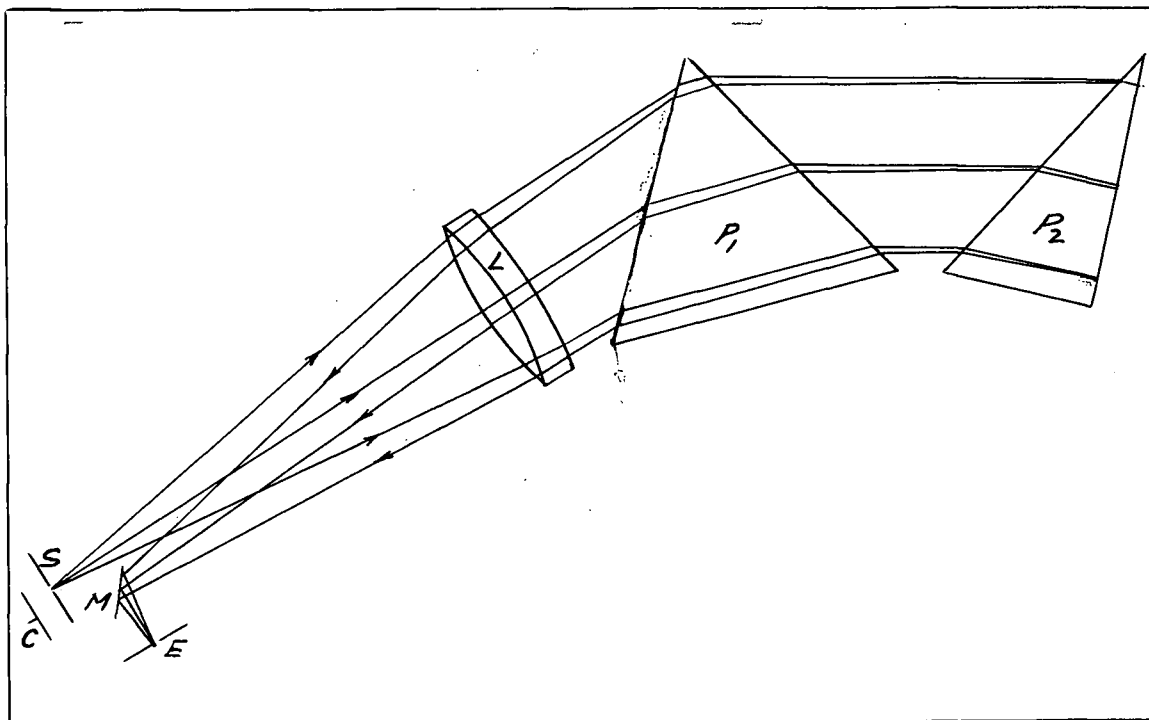


Fig. 1.2. Optical sequence (lens collimation).

Scanning was to be accomplished by rotating P_1 and P_2 in such a manner that the wave length instantaneously being under conditions of minimum deviation was the one reflected from M and passed out at E.

The incident radiation was to be chopped at 900 c.p.s., and the output of a PbS photo-conducting cell was to be coupled to a high gain, narrow-band amplifier tuned to the above fre-

quency. The resulting output was to be rectified in order to actuate the pen of a Brown Recording Potentiometer.

Calculations in subsequent chapters will show that the use of lenses for collimation is inadvisable where the scope of wave length covered is somewhat large, because of chromatic

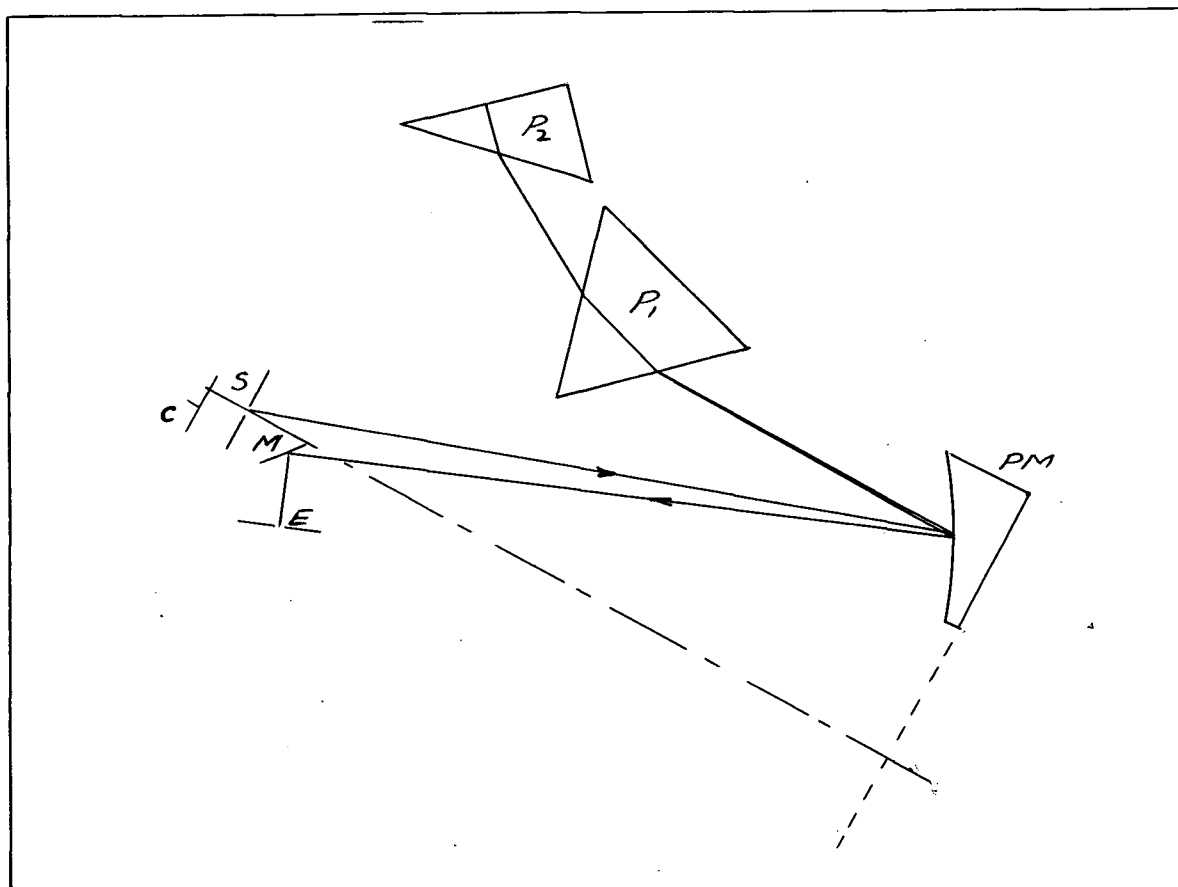


Fig. 1.3. Optical sequence (mirror collimation).

aberration and coma. At best, it necessitates a controlled motion of the slits or lenses in order to have the correct focal length for the wave length concerned.

After the original plans had been put into production, and the magnitude of Δf had been calculated, it was decided to use a 14° off-axis parabolic mirror R instead of a lens. The modi-

fication to the optical path is shown in Fig. 1.3.

Some attempts were made to use a plane grating in place of the half-prism, as it was hoped that a considerable increase in dispersion and resolving power would result. The author went so far as to devise a mounting for the grating and set up the optical sequence using a mercury arc for trials. However, he found that an excessive amount of order-overlapping occurred, (in optimum positions of prism and grating for the first order to be at minimum deviation, the green line at 5461 \AA in order $n+1$ fell on the yellow doublet $\sim 5690 \text{ \AA}$ in order n) and rather than undertake the task of setting up a complicated fore-prism or filter system, he decided to abandon the idea.

Details of the electronic sections of the spectrograph are given in Chapter 5. The photoelectric cell was mounted at the exit slit, together with the cathode-follower untuned pre-amplifier. The output from the pre-amplifier was fed through a coaxial cable to the main (tuned) amplifier, and the output from the latter rectified for input to the Brown Recording Potentiometer.

The slits, prisms, mirror, photo-cell, scanning drive, and pre-amplifier were mounted on a four inch wide-flange steel I-beam section and the whole was enclosed in a light-tight box. Details may be found in the working drawings.

CHAPTER 2

CALCULATIONS APPLYING TO THE GEOMETRIC OPTICS OF THE LIGHT PATH

A. THE PRISMS

In order to determine the absolute and relative amounts of rotation of the two prisms for the wave length range desired, it was necessary to determine the index of refraction of the glass as a function of wave length. The first (not necessarily true) assumption made was that the properties of the half-prism were the same as those of the full prism. It is a simple matter to obtain the constants A and B in the Cauchy formula for a full prism. One measures the minimum deviation angle D and uses formula 1.1 to find values of n for any two values of λ in the visible region. This may be done on a simple spectrometer consisting of source, collimator, prism table, and telescope fitted to verniers.

For the half-prism, the task requires more specialized equipment. A schematic diagram of the necessary optical system is shown in Fig. 2.4. S is the entrance slit for the system and L_1 the collimating lens. M is a half-silvered mirror which reflects the light to P_2 , and the dispersed radiation is passed through M and observed by means of the telescope T. Since, at minimum deviation, the angles of incidence and emergence in air are the same, it follows that there is only one position of P_2 for which a wave length λ will intersect the

cross-hairs of the telescope; and this will occur at minimum deviation for that wave length.

The angle of incidence may be found by noting the vernier reading when the slit is imaged in the front face of the prism and then taking the angle of rotation required to bring the particular wave length line to the cross-hairs. Then it follows

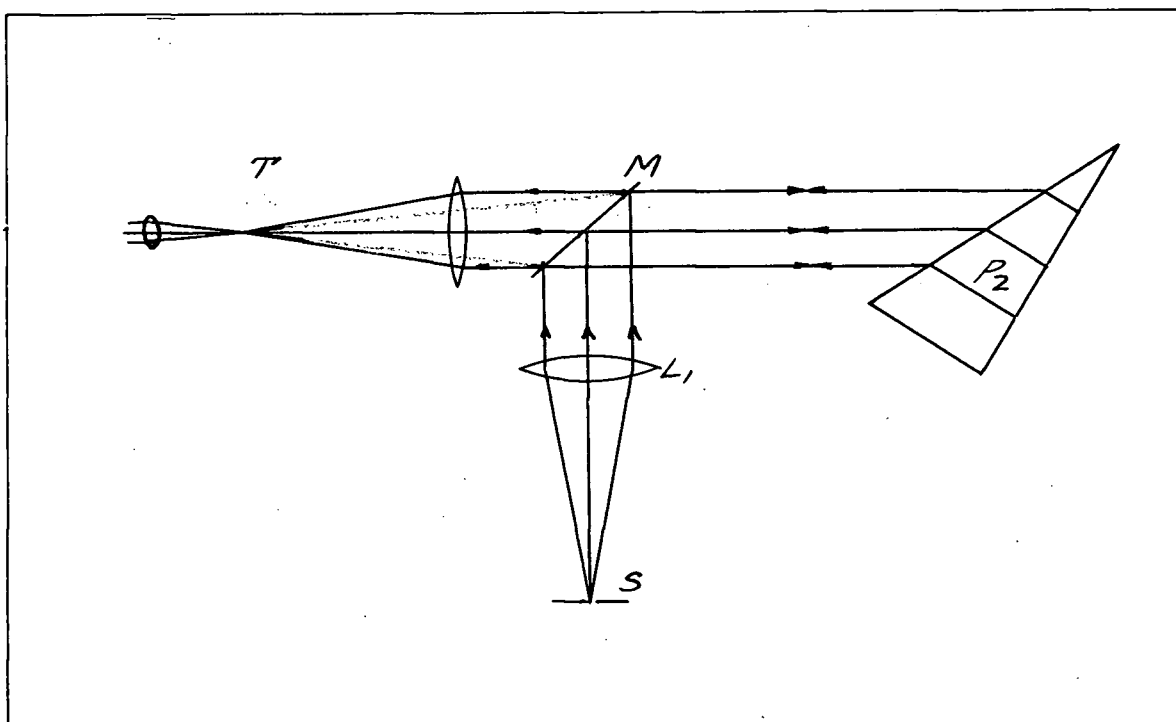


Fig. 2.4. Finding N_λ for a half-prism.

that $D = 2(i-A)$ where A is the prism angle. In the present case, the assumption that the half-prism had the same properties as the full prism did not introduce much error and reduced the number of necessary measurements.

For the measurements on the prism used in this spectrograph, a Mercury arc was used as a source and the angle of minimum deviation D was measured for various known lines in the spectrum. The results are in Table 2.1. The prism angle was found

to be $60^{\circ} 01'$ by one of several simple methods not described here.

Table 2.1. Results of measurements for the full prism.

$\lambda(\mu)$	$\frac{1}{\lambda^2}$	D	$\sin \frac{D+A}{2}$	N
0.70720	1.99948	47 08.5	0.80468	1.60897
.69075	2.09578	47 15.0	.80524	.61009
.62343	2.57286	47 33.5	.80683	.61327
.61234	2.66688	47 37.0	.80713	.61387
.60726	2.71172	47 38.5	.80744	.61449
.57907	2.98222	47 39.0	.80730	.61421
.57690	3.00472	47 40.0	.80739	.61439
.54607	3.35345	48 13.0	.81021	.62003
.49603	4.06421	48 49.0	.81327	.62615
.49160	4.13787	48 53.5	.81365	.62691
.43583	5.26454	49 56.5	.81895	.63751
.40465	6.10687	50 42.0	.82272	.64504
.39840	6.30040	50 46.5	.82310	.64580

A graph of N against $\frac{1}{\lambda^2}$ is shown in Fig. 2.4a. From two points on the straight line approximation, it was found that the constants had the values,

$$A = 1.59100$$

$$B = 0.00882\mu^2$$

The angles of minimum deviation were then calculated for wave lengths 0.4μ , 0.7μ , and 2.5μ with the following results, shown in Table 2.2.

This means that the total change in D is $5^{\circ} 15'$ if the scanning is to commence at 0.4μ (to facilitate setting up by

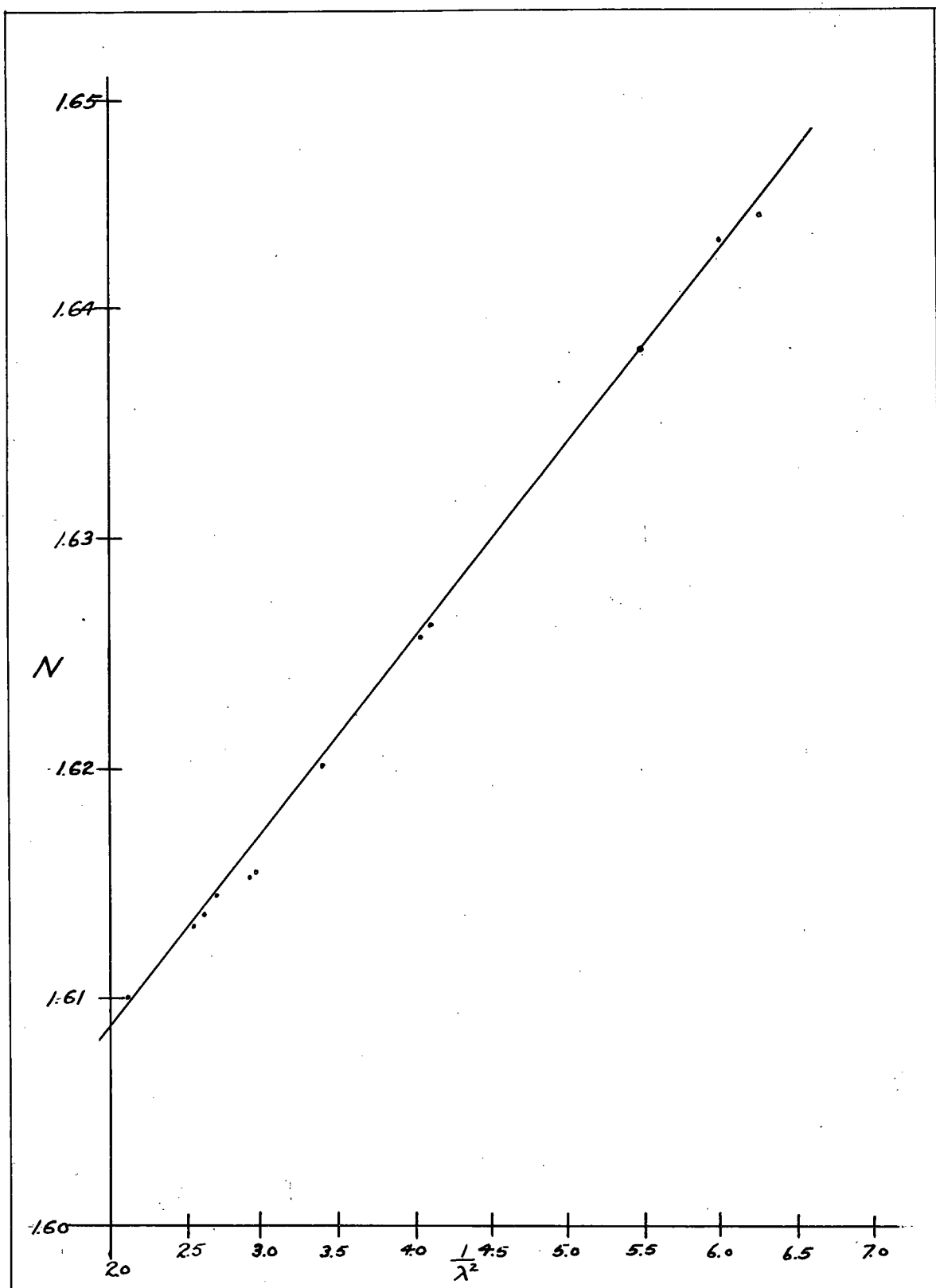


Fig. 2.4a. Graph of Index N of unknown glass against $\frac{1}{\lambda^2}$.
(λ in μ)

use of the visible region). Hence, it was required that the full prism have approximately $2^{\circ} 40'$ of rotation, approximately

Table 2.2. N and D at violet, red, and infra-red wave lengths.

$\lambda(\mu)$	N	D	ΔD
0.4	1.646	$50^{\circ} 48'$	$3^{\circ} 39'$
0.7	1.609	$47^{\circ} 09'$	$1^{\circ} 36'$
2.5	1.592	$45^{\circ} 33'$	

half of ΔD . The actual details of the prism rotation are described in the next chapter.

B. THE LENS

The lens proposed for the spectrograph was a doublet of BSC 510644 and EDF 653336, with aperture approximately 3.7 inches. The explanation of this standard nomenclature is as follows: BSC stands for borosilicate crown and EDF for extra dense flint. The first three figures in the number represent the figures after the decimal point in the refractive index at $\lambda 5890$, (NaD line), and the last three (with a decimal point before the last) the Abbé number $\frac{N-1}{dN}$.

The formation of a perfect achromatic doublet is essentially a problem of obtaining a resultant infinite Abbé number ($dN = 0$) so that there is no chromatic aberration. This is not rigorously possible even over the visible light wave lengths but can be very closely approximated. It will be shown, however, that for the lens under discussion the aberration was quite severe over the desired wave length range and would have

necessitated continual changing of the slit-lens during scanning.

In order to compute the focal length of a doublet for a range of wave lengths, it is necessary to carry out a tracing schedule either by logarithmic or machine methods, and the first requirement is that one know, for each component, the thickness, radii of curvature of faces, and indices for certain

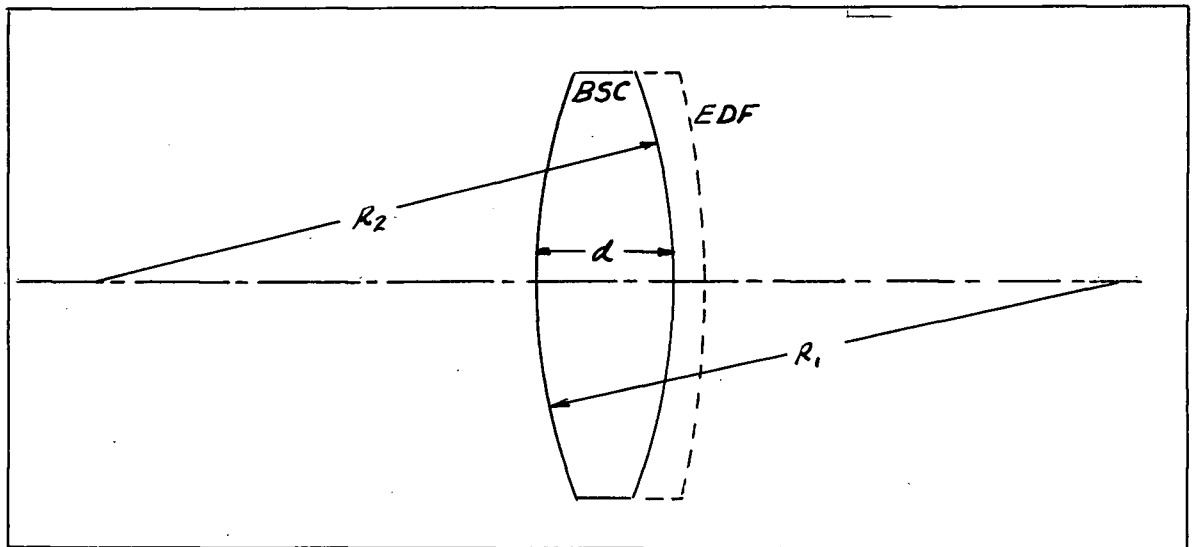


Fig. 2.5. Explanation of symbols in an achromatic doublet.

wave lengths. These quantities for the lens in question are listed in Table 2.3. (See also Fig. 2.5).

The cartesian sign convention is used throughout all calculations. Radii of surfaces concave to object space are negative and conversely. Distances of real objects and real images are positive, and distances of virtual images and virtual objects are negative.

It will be noted that the indices for $\lambda 5890$ were not those that would be expected from the code number of the glass.

Table 2.3. N_λ for the components of the achromatic doublet.

			R_1	R_2	d	
CROWN	BSC	510644	13.89"	-11.94"	0.6"	
FLINT	EDF	653336	-11.94"	-48.00"	0.4"	
$\lambda(\mu)$	CROWN	FLINT				
2.4	-	1.6131	x			
2.2	1.4886	1.6150				
2.0	1.4908	1.6171				
1.8	1.49273	1.6193				
1.6	1.49461	1.6217				x
1.4	1.49635	1.6249				
1.2	1.49832	1.6277				
1.0	1.50044	1.6315				x
0.8	1.50341	1.6373				
0.7680	1.50594	1.6382				
0.6563	1.50629	1.6444				x
0.5890	1.50960	1.64985				
0.5349	-	1.65601				
0.5086	-	1.65979				
0.4861	1.51520	1.66367				x
0.4800	-	1.66482				
0.4678	-	1.66725				
0.4340	1.51976	1.67561				x
0.3610	-	1.70536				
x - Used in tracing schedule						

This is because the indices for a series of wave lengths were not available, and those for a very similar glass¹ had to be used. ΔN_D was not large; it only occurred in the third decimal place, and the fact that the author was only interested in a change of focal length further minimized the error due to the approximation.

The author is much indebted to Dr. A. M. Crooker for the details of the ray-tracing procedure used here. The method is

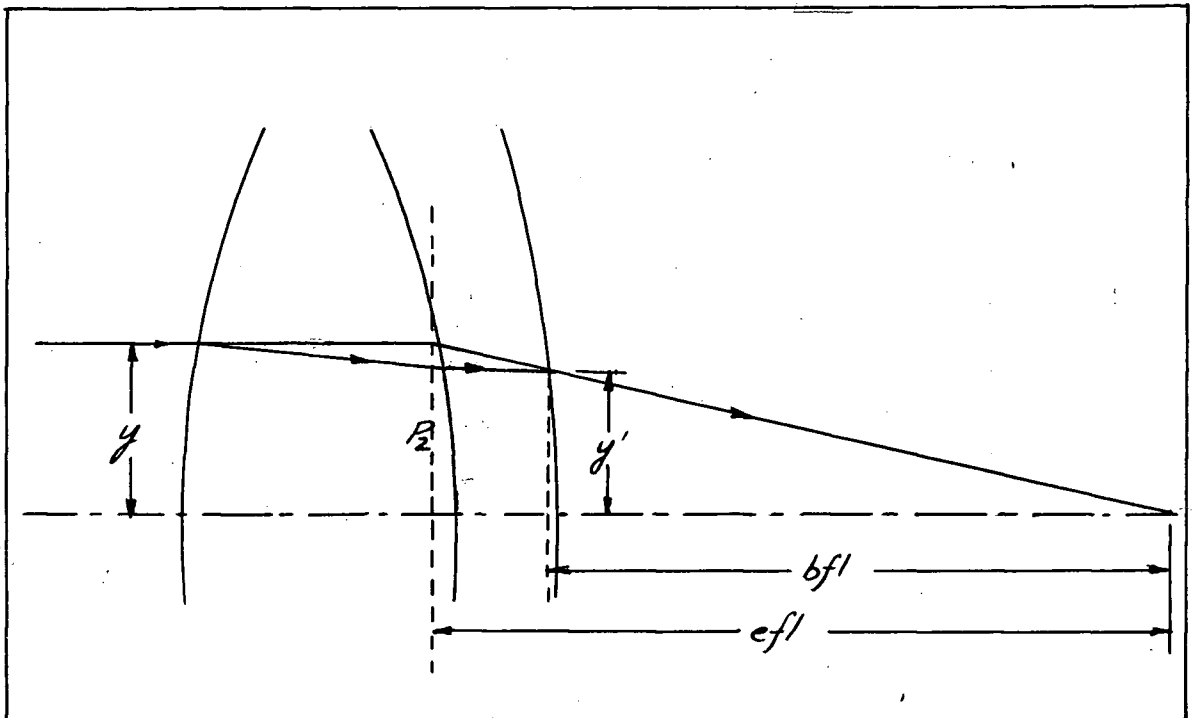


Fig. 2.6. Showing the significance of bfl and efl in paraxial ray tracing.

admirably suited for solution by calculating machine, and was adopted in its original form. For the lens in question, a paraxial and an axial trace were carried out, and the three quantities bfl (back focal-length), efl (effective focal-length),

1. H. Thiene - "Glas" - p.286.

and L' were found for wave lengths (in μ) 0.4340, 0.4861, 1.0000, 1.6000, and 2.2000. The definition of these three quantities is as follows:

The back focal-length and effective focal-length of an achromatic doublet are found from the paraxial ray (i.e. "near the axis") trace. The bfl is defined by $\frac{y'}{u}$ in Fig. 2.6 when the incident ray is parallel to the axis of the lens. It is actually the focal-length measured from the emergent face of the lens. The efl is defined by $\frac{y}{u}$ in Fig. 2.6, again when the

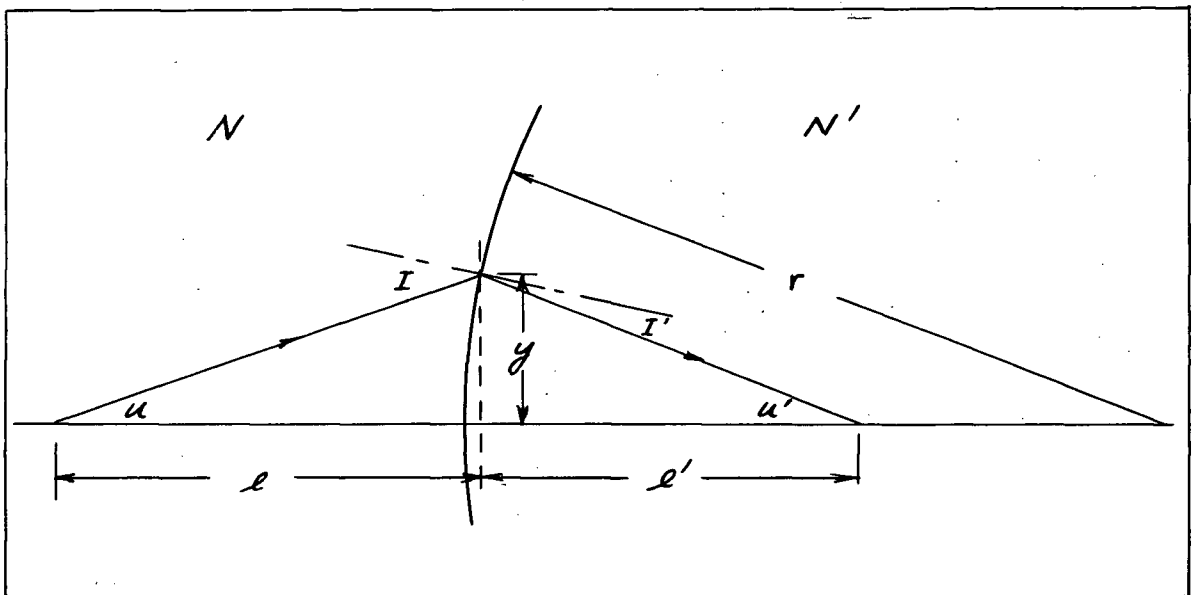


Fig. 2.7. Construction for proving the Abbé invariant.

incident ray is parallel to the optical axis, and is the focal-length measured from the second principle plane of the lens. In the paraxial trace, where one is considering very small convergent angles u , it is possible to use the angle in radians rather than its functions.

The paraxial ray trace begins with the Abbé invariant.

In Fig. 2.7, provided the angles u are small,

$$I = \frac{y}{l} - \frac{y}{r} \qquad I' = \frac{y'}{l'} - \frac{y}{r}$$

$$\therefore N \left(\frac{y}{l} - \frac{y}{r} \right) = N' \left(\frac{y'}{l'} - \frac{y}{r} \right) \quad (\text{Abbé invariant})$$

or, if $\frac{y}{l} = u$ (the convergent angle)

$$N'u' = Nu + \frac{(N' - N)y}{r} \quad (2.1)$$

2.1 gives $N'u'$ for a given Nu in terms of definite lens constants. The transfer formula for proceeding from one lens surface to the next is simply,

$$y_2 = y_1 + \left(-\frac{d}{N} \right) Nu \quad (2.2)$$

where d = thickness of first medium.

These two formulae can be arranged in a "staggered paraxial" tracing schedule that is very fast.

The results of the application of this method to the lens in question, together with the calculation of the two characteristic focal-lengths, are compiled in Table 2.4.

The values of L' are found from an axial ray trace. In this schedule the angles of incidence, refraction, and convergence are calculated, as well as the perpendicular distance, Q , from the lens vertex onto the ray being traced. Quite arbitrarily, a ray distant 0.8 of the radius of the lens from the axis is considered. L' is the focal length for these axial

rays, and is defined in exactly the same way as bfl in the paraxial trace. The difference between bfl and L' at any wave length is a measure of spherical aberration, that is, the variation with y of the focal length.

From the geometry of Fig. 2.8,

$$Q = r(\sin U + \sin I) \quad 2.3$$

which serves as an opening equation to calculate I given $U = 0$

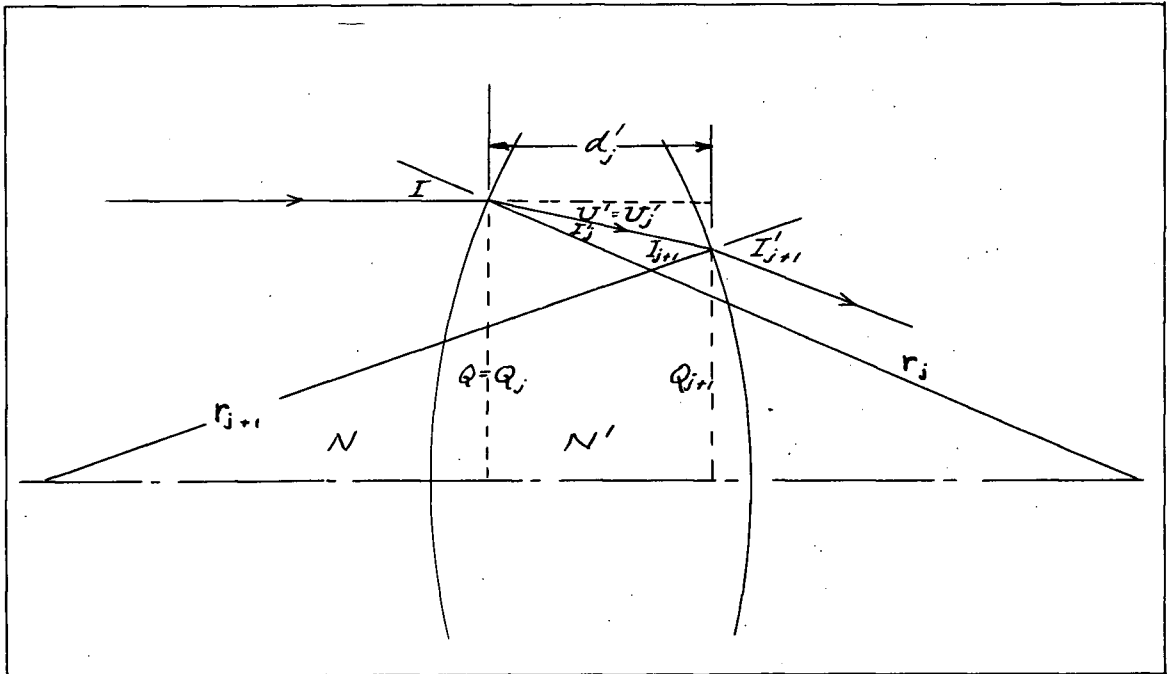


Fig. 2.8. Axial ray trace parameters.

for an infinite object and Q = opening paraxial y . From Snell's law,

$$\sin I' = \frac{N}{N'} \sin I \quad 2.4$$

and from the geometry,

$$U' = U + I - I' \quad 2.5$$

then 2.3 transferred gives

$$Q' = r(\sin U' + \sin I') . \quad 2.6$$

The transfer equation from one surface to the next is

$$Q_{j+1} = Q_j' - d_j' \sin U_j \quad 2.7$$

From $\sin I$ and I calculated from 2.3, one calculates $\sin I'$ and I from 2.4 and the transfer to the following surfaces is made by the following,

$$\sin I_{j+1} = \frac{Q_{j+1}}{r_{j+1}} = \sin U_j' \quad 2.3A$$

$$= \frac{Q_j'}{r_{j+1}} - \frac{d_j' \sin U_j'}{r_{j+1}} - \sin U_j'$$

$$= \frac{r_j \sin U_j'}{r_{j+1}} + \frac{r_j \sin I_j'}{r_{j+1}} - \frac{d_j \sin U_j'}{r_{j+1}} - \frac{\sin U_j' r_{j+1}}{r_{j+1}}$$

$$= \frac{r_j \sin I_j' + C_j' \sin U_j'}{r_{j+1}} \quad 2.8$$

$$\text{where } C_j' = r_j - d_j - r_{j+1}$$

The closing equation is

$$L' = \frac{Q'}{\sin U'} \quad 2.9$$

The results of this calculation for the lens in question

Table 2.5. Axial ray trace of BW 19/20.

Opening axial $y = 1.3''$			
	Crown	Flint	
r''	13.89	-11.94	-48.00
d''	0.6	0.4	
N	1.51976	1.67561	
"C"	25.23	35.66	
sin U	0.032102	0.019017	0.049861
U	1.83961	1.08966	2.857990
sin I	0.093593	-0.139474	-0.045595
sin I'	0.061584	-0.126502	-0.076400
I	5.37032	-8.01743	-2.61333
I'	3.53071	-7.26748	-4.38166
$\lambda = 4340\text{\AA}, \quad Q' = r(\sin U' + \sin I) = 1.273891''$			
$L' = Q'/\sin U' = 25.5490''$			
r''	13.89	-11.94	-48.00
d''	0.6	0.4	
N	1.50044	1.6315	
"C"	25.23	35.66	
sin U	0.031308	0.020068	0.049560
U	1.79408	1.14986	2.84076
sin I	0.093593	-0.138719	-0.046643
sin I'	0.062377	-0.127575	-0.076098
I	5.37032	-7.97371	-2.67340
I'	3.57624	-7.32949	-4.36430
$\lambda = 1\mu, \quad Q' = r(\sin U' + \sin I) = 1.273795''$			
$L' = Q'/\sin U' = 25.701926''$			

Table 2.5. - Continued.

	Crown	Flint	
r''	13.89	-11.94	-48.00
d''	0.6	0.4	
N	1.49461	1.6217	
"C"	25.23	35.66	
$\sin U$	0.031064	0.020116	0.049192
U	1.78011	1.15270	2.81965
$\sin I$	0.093593	-0.138487	-0.046693
$\sin I'$	0.062620	-0.127634	-0.075723
I	5.37032	-7.96029	-2.67631
I'	3.59021	-7.33288	-4.34326
$\lambda = 1.6\mu, Q' = r(\sin U' + \sin I) = 1.273459$			
$L' = Q'/\sin U' = 25.88736$			
r	13.89	-11.94	-48.00
d	0.6	0.4	
N	1.4886	1.6150	
"C"	25.23	35.66	
$\sin U$	0.030811	0.019898	0.048519
U	1.76560	1.14012	2.78100
$\sin I$	0.093593	-0.138246	-0.046479
$\sin I'$	0.62873	-0.127426	-0.075062
I	5.37032	-7.94635	-2.66403
I'	3.60472	-7.32087	-4.30491
$\lambda 2.2\mu, Q' = r(\sin U' + \sin I) = 1.274189$			
$L' = Q'/\sin U' = 26.2619$			

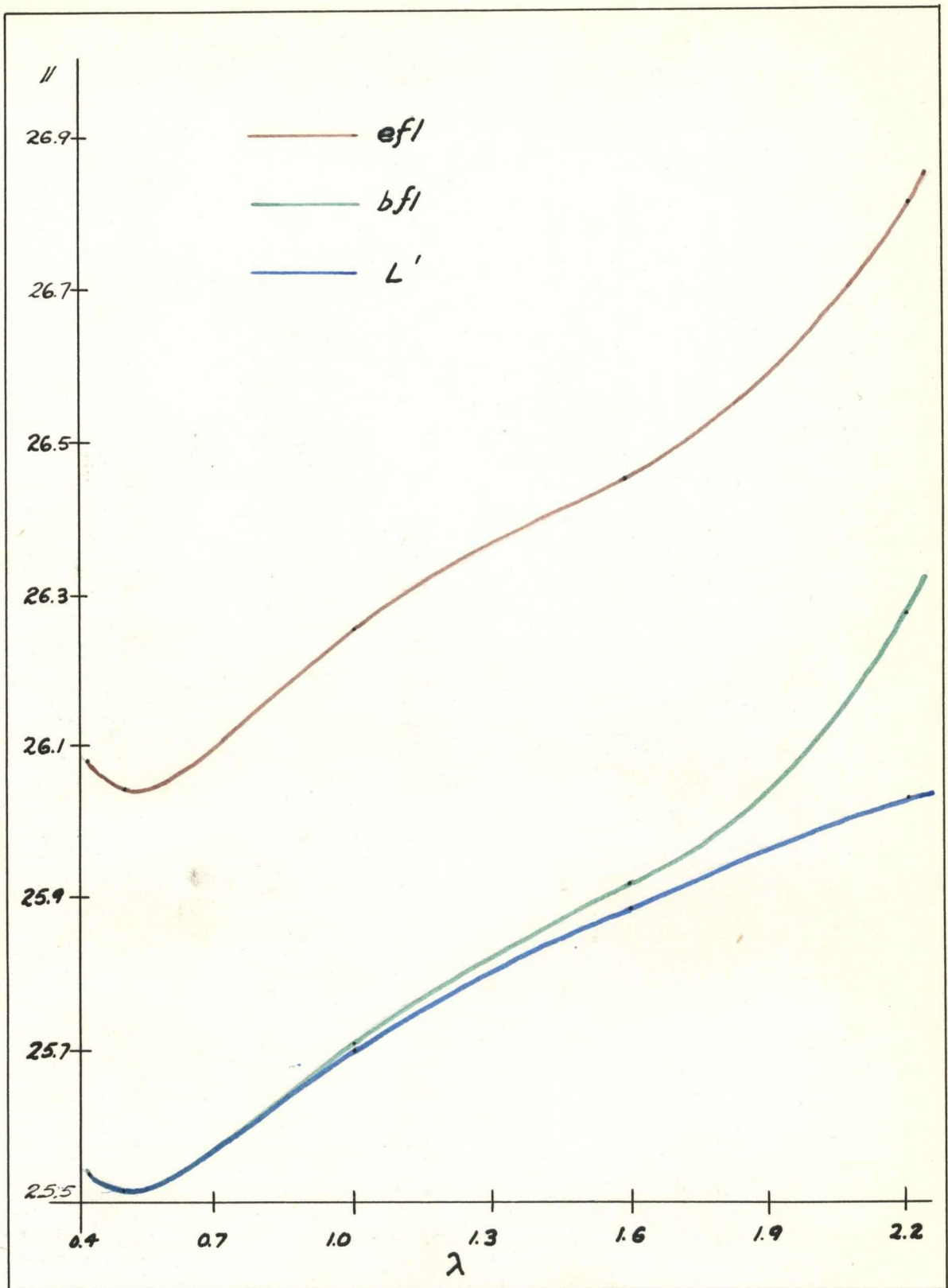


Fig. 2.9. Variation of bfl , efl , and L' with λ .

(λ in μ)

are shown in Table 2.5, for the same series of wave lengths as in Table 2.4.

Fig. 2.9 shows graphically the variation of bfl , efl , and L' with wave length. It will be noticed that none of these values is a linear function of wave length, and in the vicinity of 0.5μ each curve has a minimum. Also, spherical aberration is much increased in the infra-red, and indications are that conditions in this regard deteriorate as λ is increased. For these reasons, it was decided to dispense with the lens for the

Table 2.6. Theoretical resolving power of the spectrograph for certain wave lengths.

$\lambda(\mu)$	N	$d\theta/dN$	$dN/d\lambda$	R.P. = $a \frac{d\theta}{d\lambda}$
0.4	1.646	1.976	0.276	43,273
1.0	1.600	1.667	0.018	2,382
1.6	1.594	1.656	0.004	556
2.0	1.593	1.653	0.002	238
2.5	1.592	1.650	0.001	159

project and use instead a 14° off-axis paraboloid of focal-length one metre.

The amount of rotation required for the full prism has already been shown. The theoretical resolving power for the final optical sequence was then calculated from equations 1.2, 1.4, and 1.5 of Chapter 1 and results for various λ are shown in Table 2.6.

The theoretical resolving power as defined by $\lambda/\Delta\lambda$ is seen to be increasingly poor as one goes into the infra-red.

As will be shown in a later chapter, the actual resolving power obtained was better than the calculated value. Certainly there is no guarantee that the Cauchy formula is valid over a large range of wave lengths; and in view of the fact that the $\frac{dN}{d\lambda}$ term (which influences the resolving power greatly) depends on the $N - \lambda$ relationship, one might expect a difference between the theoretical and observed values of $\frac{\lambda}{d\lambda}$.

CHAPTER 3

THE PRISM TABLE AND SCANNING DRIVE

A. INTRODUCTION

In this chapter and the following, the scope and solution of the mechanical problems encountered will be discussed. It was necessary to spend considerable time on sketching and drawing in order that every component in the final apparatus would be correctly positioned with respect to all others. Further, it was imperative that all moving parts function very smoothly and at the same time cause no undue load on the driving mechanism; and also that the entire assembly be as vibration-proof as possible. For a detailed study of the working drawings, the reader is referred to Appendix A. For the present, a schematic diagram is included in the text where it is felt that one will clarify the description of the particular part in question.

B. ROTATION OF THE PRISM TABLE

Consider the condition where the prisms are set to contain a given wave length at minimum deviation. If now it is required to rotate all prisms so that another wave length is at minimum deviation, and the change in angle of deviation is ΔD , this means that the full prism must rotate $\frac{\Delta D}{2}$ and the half prism $\frac{3\Delta D}{2}$ in the same sense. Reference to Fig. 3.10 will show how this condition was achieved. A solid cylinder was fitted to the main spectrometer beam, and had fixed to it, axially, the outer races of two bearings and a 4" pitch diameter spur

gear. The shaft fitted to the bearings carried at its upper end an aluminum table, and over the axis of rotation the full prism was rigidly fixed so as to turn with the table. The aluminum table carried, in a yoke, the outer races of two bearings which, in turn, carried a shaft fitted with a smaller circular table and a 2" diameter spur gear. The half-prism was rigidly clamped to the small table, and hence turned with the smaller gear; and the spacing of shafts was such that the two spur gears were in mesh.

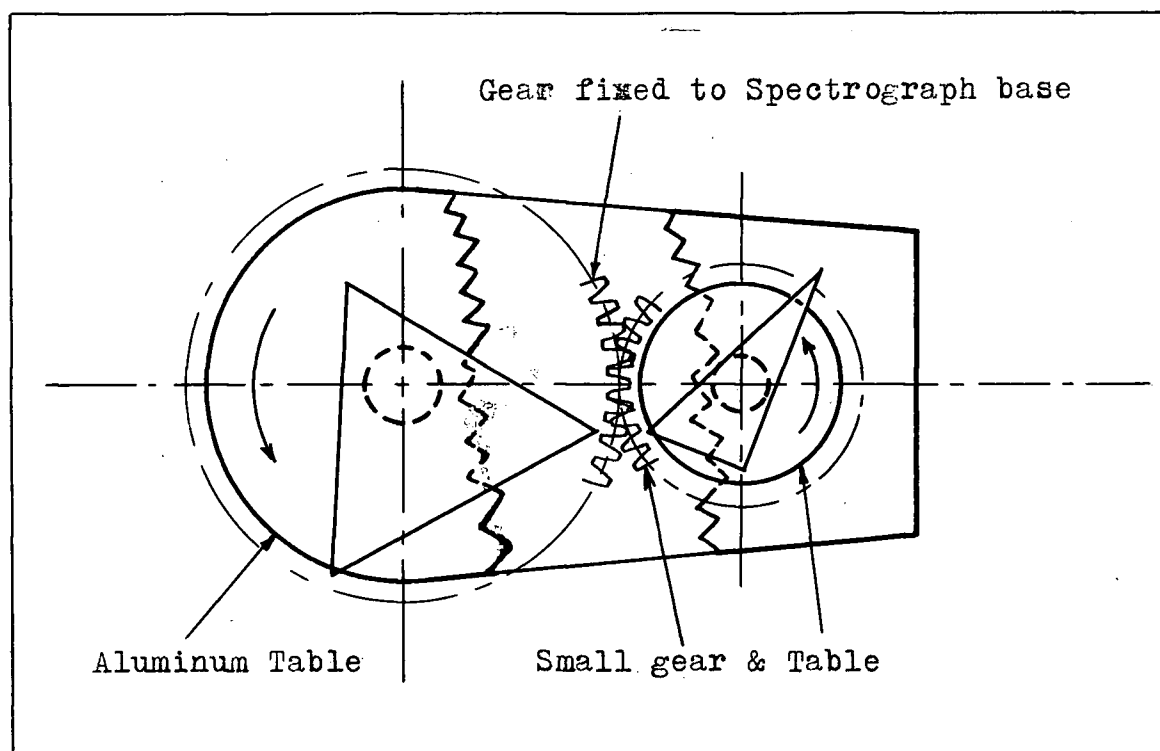


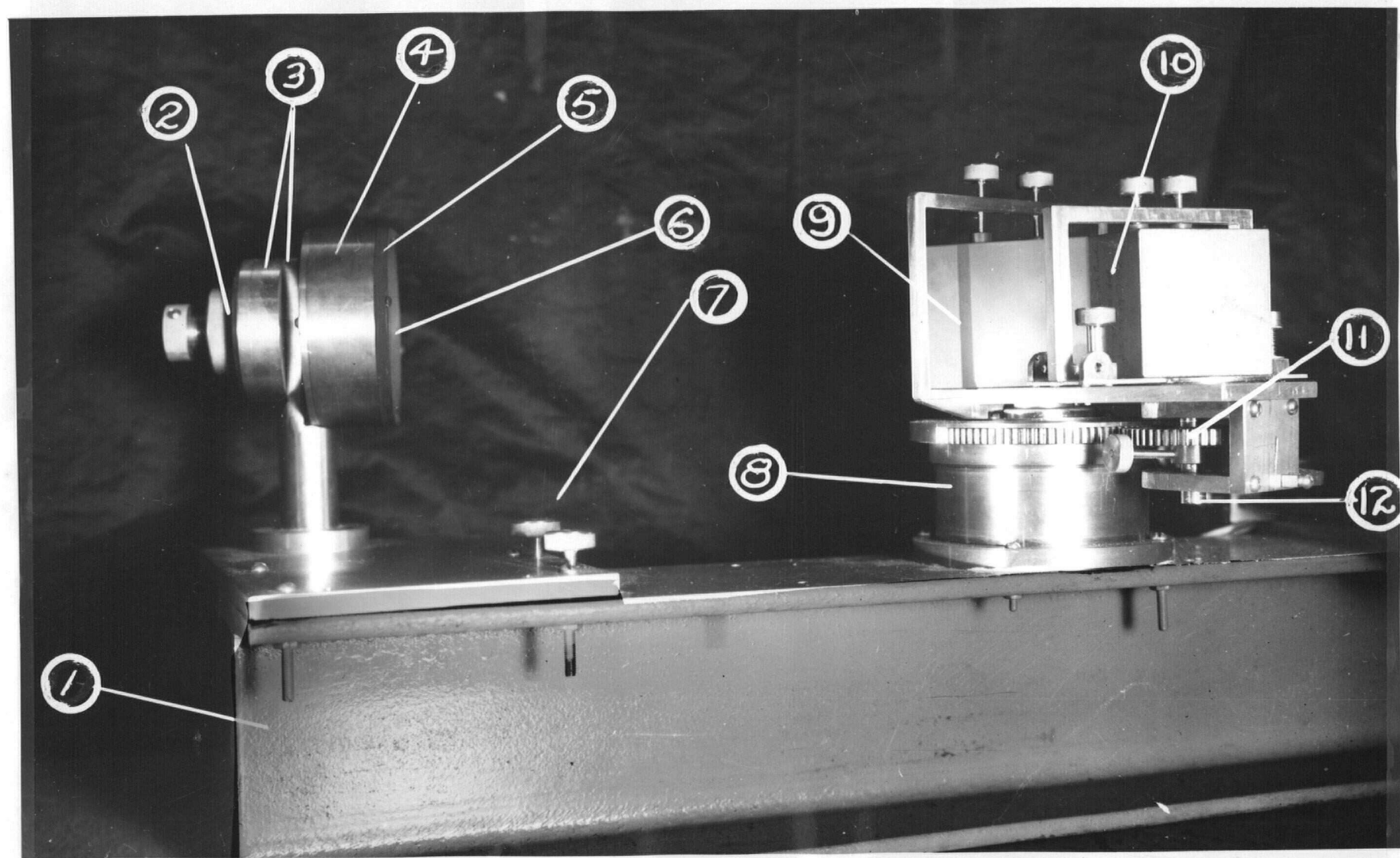
Fig. 3.10. Prism Table.

Suppose, now, that the direction of incident radiation is fixed. In order to accept different wave lengths at minimum deviation, it was necessary to rotate the large prism table and its prism about the large gear, and by virtue of the diameter

PLATE I

THE PRISM TABLE AND MIRROR ASSEMBLIES

1. Main base
2. Locking ring
3. Mirror support
4. Mirror cell
5. Retaining ring
6. Mirror
7. Adjustment screws
8. Prism table base
9. Full prism
10. Half prism
11. Small gear
12. Small table shaft



ratio of the two gears, the small table and its associated half-prism were turned the proper relative amount. That is, if the large prism table turned through Θ , (with respect to the large gear) then the small table would turn through 2Θ with respect to the large and hence through the desired 3Θ with respect to the spectrometer base.

It will be noticed that, in this arrangement, light of only one wave length travels parallel to the large table, and for all other wave lengths, (at minimum deviation) there is a slight divergent angle - Θ , to be exact. This was not important, since the dimensions of the prisms were adequate to ensure complete filling of the prism optics for all wave lengths; therefore it was decided to clamp the two prisms in such a position that λ 5690 at minimum deviation would be parallel to the large table and all other wave lengths would deviate slightly.

C. THE SCANNING DRIVE

Provision was made for two speeds of scanning that portion of the spectrum under consideration. The entire range was to be covered in roughly twenty minutes at slow speed, and in ten seconds at high speed. This immediately excluded from any consideration a driving mechanism wholly dependent on gears or worm gears, since the necessary ratio of speed would be 1:120 and would be impossible to achieve from any constant speed driving motor. Furthermore, the slow speed scan would only be possible through a worm drive and this would necessitate scanning for both increasing and decreasing wave lengths (hence two

calibrations) and require reversibility of the motor. Also, any mechanism capable of being reset at will would be extremely complicated. Most important, such a direct motor-to-prism table drive would have considerable backlash and vibration directly proportional to the number of rotating parts.

The method finally used permitted scanning only in the direction of increasing wave length and was as follows: the motor was a 2 R.P.M. telechron synchronous, and drove one of two shafts by a simple gear selection device. One shaft, driven by a 3:1 gear ratio at 6 R.P.M., was to drive another shaft carrying a cam. The other, driven by a 4:1 gear ratio, was to rotate at $\frac{1}{2}$ R.P.M. and turn a micrometer screw. By means of a spline clutch, the micrometer was able to move ahead in its yoke (fixed to the same base as the motor) while rotating at this slow speed.

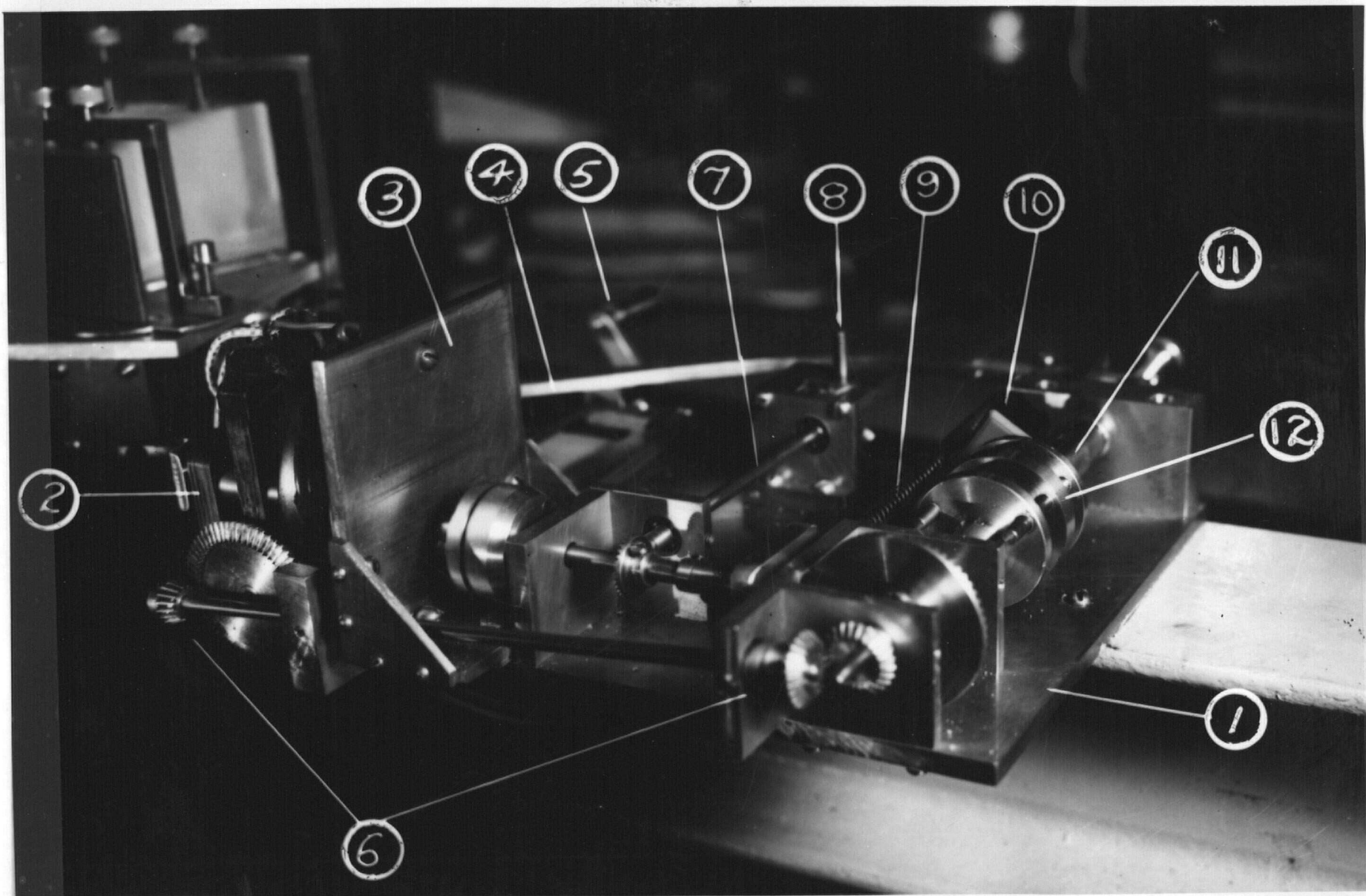
A long lever arm, fixed to the prism table, was constrained by a spring to bear against the end of the micrometer, so that the rotation of the latter and its consequent slow movement axially caused the prism table and its components to rotate. To carry out a high speed scan, it was only necessary to retract the micrometer with a manual returning drive and then couple the motor to the cam, which bore against the lever arm.

Supposing that the required angle of rotation was $2^{\circ} 30'$, and considering the fact that the prism table lever arm gave an effective throw radius of approximately 15 inches, this meant that the micrometer had to travel linearly about 0.6 inches or 15 mm. On this micrometer, one revolution was equivalent to

PLATE II

THE DRIVING MECHANISM

1. Drive base plate
2. Motor
3. Motor mount
4. Prism table lever arm
5. Manual return crank
6. Manual return gears
7. Cam drive shaft
8. Cam shaft
9. Prism table return spring
10. Automatic stop switch
11. Micrometer
12. Spline clutch



0.5 millimeters, so that 30 revolutions (and one hour) would be required for the complete scan. This time is considerably over-estimated, because scanning would never start in the extreme violet and the range from 0.4μ to 0.6μ would take up nearly one third of the time due to the dispersion properties of the optical parts.

It was planned, in the high speed scan, to put the amplifier output onto the screen of a high-persistence cathode ray oscilloscope so that a continual spectral picture would appear. In order to avoid crowding at long wave lengths, then, it was desirable to design the cam so that the prism table rotated rapidly in the visible and slowly in the infra-red so that the pattern would be linear on a wave length scale.

If one assume that the Cauchy formula is valid over the range of wave lengths being considered, then it is possible to derive the following formula for r , the radius of the cam, in terms of r_0 , (minimum radius) l , (prism table lever radius) and Θ , (angular rotation of cam from Θ_0).

$$r = r_0 + \left[57^\circ 09' - \arcsin \left\{ 0.8124 + \frac{0.00443}{(0.4 + \frac{2.1\Theta}{\pi})} \right\} \right] l \quad 3.1$$

Since the form of the dispersion variation was not definitely known, it was decided not to construct a cam based on these calculations. With the advice of Dr. Crooker, the author decided to abandon the cam drive and concentrate on obtaining satisfactory results with the slow scan. As will be seen later, the speed of response of the PbS photo-cell is such that no line

structure would have been observable with high speed scanning; and the only useful purpose thereof would be in getting an overall picture of the response of the spectograph to a source of continuous radiation such as a Nernst glower or a black body.

CHAPTER 4

THE MIRROR AND THE SLITS

A. THE OFF-AXIS PARABOLOID

This requires very little description. The mirror rests against a flange at the end of a brass tube and is retained by a lucite ring at the front. The latter is blackened with a charcoal paint in order to avoid any passage of light through it and onto the mirror.

The mirror cell so formed is fitted axially to a shaft so that it may rotate in a plane perpendicular to the base of the mirror mount, and the angle of inclination of this plane is set by adjustment screws bearing against the main base of the instrument. Rotation of the mirror about the above mentioned axis is effected by loosening the locking ring at the back of the shaft and turning to the desired position.

B. THE EXIT SLIT MIRROR

This is the small mirror that is inclined at 45° to the returning beam of light and reflects it out through the exit slit. It is so positioned that the distance from any point on the mirror to the exit slit is exactly that from the same point to the plane of the entrance slit. It is supported in a cut-away cylinder so that the front (reflecting) surface lies along the axis of the cylinder, and is slightly adjustable as to inclination. The cylinder is pivoted at both ends in adjustable cone bearings and rotation of it is effected by a tangent screw

and spring return. The inclination adjustment enables the operator to set the image of the entrance slit exactly parallel to the exit slit. The rotational adjustment enables the operator to ensure that the light strikes the optimum portion of the photo-cell, which is spaced a little back from the exit slit so that the sensitized surface will be filled with light.

C. THE SLIT MECHANISM

The entrance and exit slits were so constructed that their mid-points were at the same height above the bed of the spectrograph as the centres of the mirror and prism train. Each slit was approximately one inch long, and the rectangular diaphragm fitted to each stopped the transmitted light beam down to $\frac{3}{4}$ ". This was entirely adequate to fill the sensitized portion of the photo-electric cell, the latter having little more than a length of one millimeter.

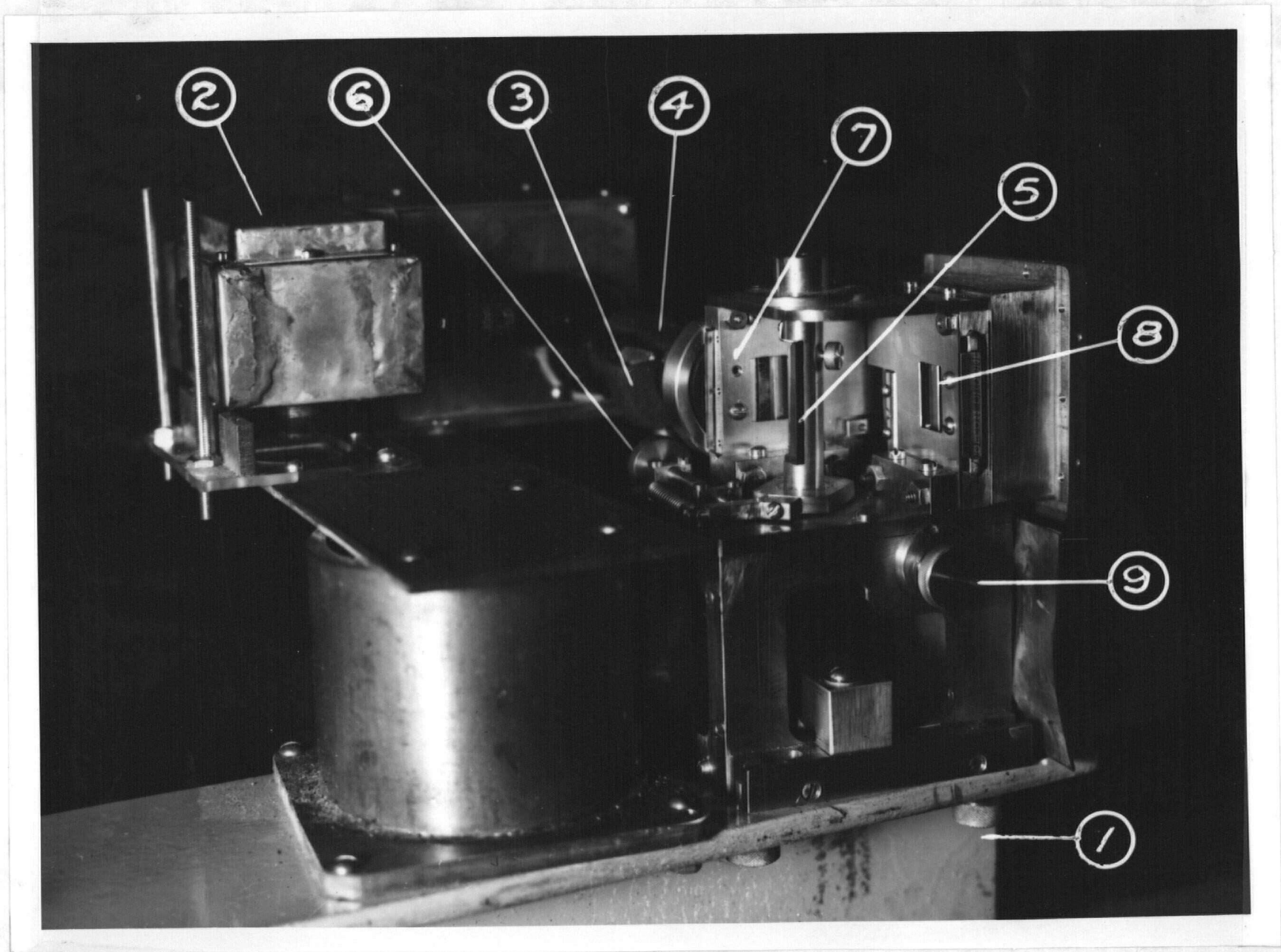
Each slit consisted of six main parts. Clamped between two cover plates (acting also as the diaphragm) were two "V" channels, (See Fig. 4.11) which acted as guides for a flat plate carrying the moveable slit jaw. The plate carrying the fixed jaw was bolted to one cover plate; and each slit jaw was fitted to its plate by oversize bolt holes to allow adjustment for parallelism.

The moving plates of each slit were extended forward and had downward projecting lugs riding in eccentric slots on the adjustment cam. This cam rotated in bearings fitted to a solid frame, which in turn served the dual purpose of giving the slits the necessary height and providing pivots for the adjust-

PLATE III

THE PRE-AMPLIFIER, PHOTOCELL, AND SLITS

1. Main base
2. Pre-amplifier
3. Photocell clamp
4. Photocell
5. Exit slit mirror
6. Exit slit mirror adjustment
7. Exit slit
8. Entrance slit
9. Slit adjustment wheel



ment cam and adjustable thumb wheel.

In the final assembly, the two complete slit mechanisms were at right angles to one another and so positioned that both were closed for one position of the adjustment cam. Rotation of the thumb wheel then turned the adjustment cam through a worm drive, and the projecting lugs with their slit jaws were pulled toward the cam axis by the eccentric slots. By virtue

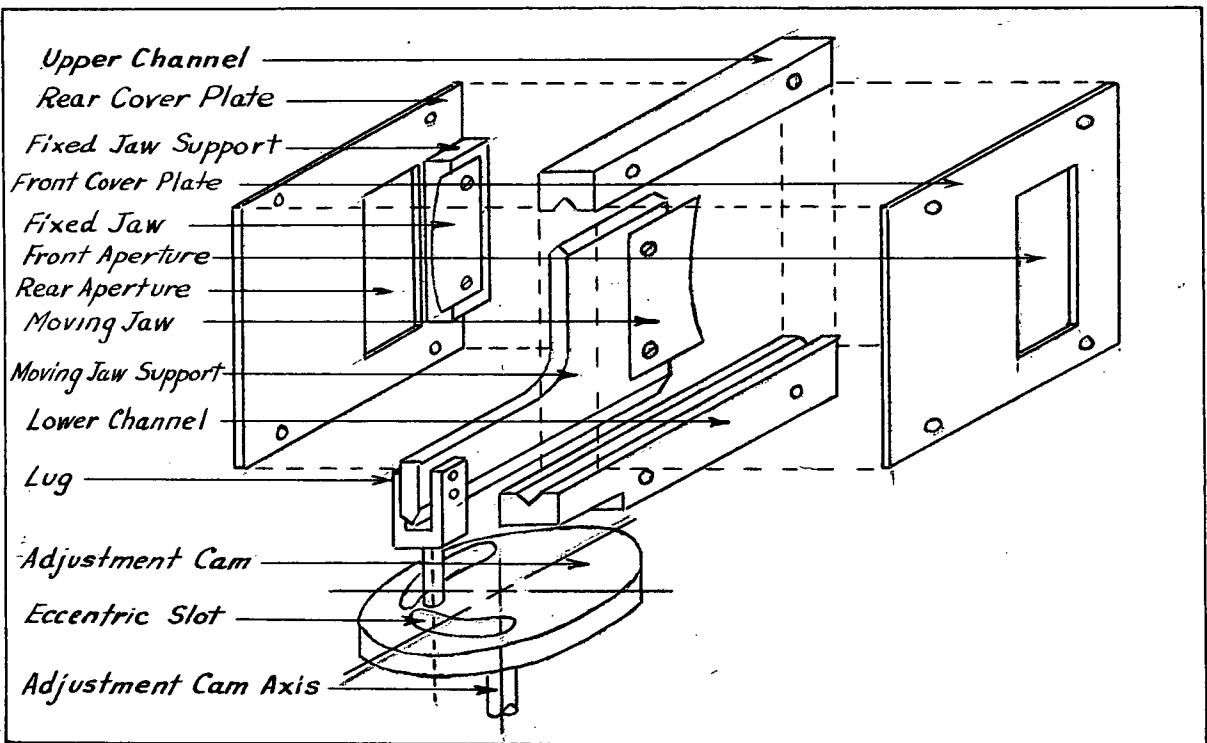


Fig. 4.11. Typical Slit.

of the slots being of equal eccentricity, the jaws were constrained to open equal amounts.

D. THE SLIT JAWS

In any prism spectrograph, there is a curvature of the image of the slit after dispersion. This is because light rays from the extremities of the slit are inclined (in a vertical

plane) after collimation, and strike the prism at an incident angle greater than does the light ray from the middle of the slit. That is, these extreme rays are deviated more, and hence displaced toward the more refracted wave lengths, i.e. toward the violet. Thus all monochromatic images of the slit are convex toward the red, and the radius of curvature is given by²

$$r = \frac{fn \sqrt{4 - n^2}}{2q(n^2 - 1)} \quad 4.1$$

where f = focal length of collimator, n = index of prism glass at the wave length concerned, and q = number of prisms. Now $r = 0$ at $n = 2$, and since the index of glass lies between 1 and 2, the radius of curvature in this spectrograph has always the same sign. For 0.4μ , $n = 1.646$, so with $f = 100$ cm., $r = 18.2$ cm. For 2.5μ , $n = 1.592$ and $r = 20.8$ cm.

As a compromise, it was decided to make the radius of curvature of the exit slit 19.5 cm., or approximately 8 inches. The entrance slit jaws were relatively easy to make. The material (discarded razor blades) was clamped between two heavy plates with plane edges and then ground to a typical slit wedge-shape. The exit slit presented more of a problem, since one jaw was concave and the other convex and the curvature of each had to be exactly the same. The method finally adopted served the dual purpose of ensuring equal curvature and also provided the wedge-shaped knife edge to each jaw.

The material for the blades was clamped between two equi-

2. Czapski & Eppenstein - "Grundzüge der Theorie der Optischen Instrumente" - p. 332.

angular hard steel cones as shown in Fig. 4.12 and the whole ground off flat on the face A-A. It can be seen that the material, on being released, will present a wedged spherical edge; and that the curvature will be the greater as the cone angle is increased. The arc so ground is not an arc of an ellipse, (undesirable) but is an arc of a circle characteristic of the development of a truncated cone.

The desired cone angle can be found by the following construction, also shown in Fig. 4.12. Suppose the jaw length is

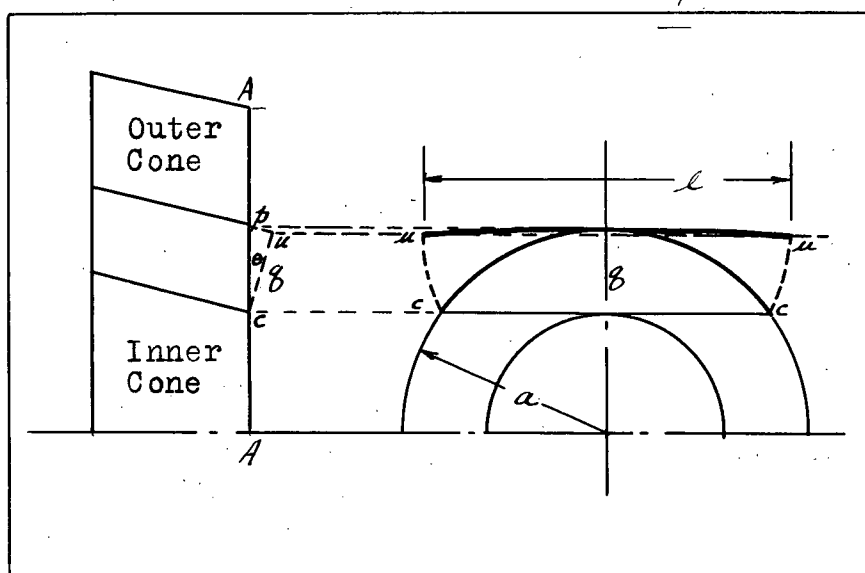


Fig. 4.12. Exit slit jaws: construction.

l, the mean radius of the cone a, and the desired slit radius of curvature r. When the material is clamped,

$$q \cong a - \sqrt{a^2 - \left(\frac{l}{2}\right)^2} \quad 4.2$$

After grinding, when the material is released, the extremes of the jaw move from c-c to u-u, and of necessity:

$$p \cong r - \sqrt{r^2 - \left(\frac{l}{2}\right)^2} \quad 4.3$$

that is,

$$\sin \Theta \simeq \tan \Theta \simeq \frac{p}{q} \quad 4.4$$

Expanding the expressions for p and q binomially, one obtains

$$\sin \Theta \simeq \tan \Theta \simeq \frac{a}{r} \quad 4.5$$

In this case, $a = 2''$, $r = 8''$, whence $\Theta = 14^\circ$.

CHAPTER 5

ELECTRONIC COMPONENTS

A. INTRODUCTION

In this chapter, the electronic sequence is reviewed. Although the chopping wheel and motor are not, by nature, electronic, they are considered in this section since this unit, in effect, serves to prepare the light beam for detection.

The discussion and description of the final spectrograph assembly is postponed until the next chapter so that all optical, mechanical, and electronic components may be considered together.

B. THE PHOTOELECTRIC CELL

This is discussed first since the design of all other components must be based on the characteristics of the photoelectric cell. Since this detector has a high speed of response, it is possible to use a fast chopping rate (usually well above 100 c.p.s.) with a consequent increase in amplifier stability for a given gain. In general, the difficulty in obtaining stability increases as the frequency decreases. By using a narrow-band tuned amplifier, it is possible to increase the signal-to-noise ratio and hence the threshold of detection by decreasing the band width, since only the noise components within the pass-band will be amplified together with the signal. However, the sharpness of tuning is limited, in practice, by the fact that the time lag increases with decreasing band width and thus some kind of compromise must be reached which will depend on the

nature of the radiation and desired speed of scanning.

For frequencies much below 100 c.p.s., the amplifier known as the "twin T" is useful. By means of sharply tuned filters, negative feedback is applied to the input except at a particular frequency, where the gain is not nullified. At higher frequencies, better results are obtained from parallel resonant inductance-capacity tuning, and the band width may be decreased by the use of more identically tuned stages or else by positive feedback to a single tuned stage. The latter is preferable since only one tuned circuit need be peaked.

The photoelectric cell used in this spectrograph was manufactured by the British Thomson - Houston Company and its pertinent specifications are given in Table 5.7. It was finally decided to use a chopping frequency of 900 c.p.s., this being the most convenient compromise in consideration of available synchronous motor speeds and the size of the chopping wheel. The photoelectric cell was fixed at the exit slit with the sensitized surface parallel to the slit, and was adequately spaced from the latter by the front cover plate. In this position, the width of the beam was sufficient to fill both sensitized surfaces. The cell was thus in a horizontal position, was supported at roughly its mid-point by a clamp fixed to the base member, and aligned by an annular ring fixed to the front cover plate. Details may be found in the working drawings.

C. THE CHOPPING WHEEL AND MOTOR.

The only synchronous motor available was a Bodine type NSY 55 rated at 1800 r.p.m., which necessitated 30 holes on the

periphery of the chopping wheel to achieve the desired 900 c.p.s. chopping rate. For convenience, the chopper was placed in front of the entrance slit. This choice of position raised the

Table 5.7. Excerpts from data sheet.
Lead Sulphide Cell Type C.

The sensitive deposit is formed on the inner re-entrant portion of a small Dewar flask. The sensitive area comprises two similar 10 x 1 mm. elements, 1 mm. apart, with a common central electrode. The sensitivity is increased about 10 times upon cooling with solid CO₂.

	<u>Operating Data</u>	
	Room Temp.	-20°C
Resistance per element	50K - 200K	500K - 2M
Optimum polarising current	100 - 150 μ amps.	50 - 100 μ amps.
Optimum interruption frequency	1000 - 2000 c.p.s.	500 - 1000 c.p.s.
Wave length of maximum sensitivity	2.2 μ	2.8 μ
Detection limit at maximum sensitivity	5 x 10 ⁻¹⁰ watt	1 x 10 ⁻¹⁰ watt
Wave length range for 10% of max. sens.	0.5 - 3.0 μ	0.5 - 3.5 μ

problem of the physical size of the motor interfering with the location of light sources, so it was decided to remove the motor from the vicinity, mount the chopping wheel on a separate shaft, and connect the two by a flexible cable. Originally, the chopper base was mounted on rubber pads on the spectrometer box. Later, changes were necessitated which are described in Chapter

6, together with the reasons for such changes. Details of the chopping wheel mounting may be found in the working drawings. The holes in the chopping wheel were $5/8$ " in diameter and the wheel was designed to be of maximum possible size without its rim reaching below the spectrometer base.

D. CHOICE OF AMPLIFIER: THE PRE-AMPLIFIER

Many references were consulted in the choice of a suitable amplifier, the one finally adopted being due to E. B. Wilson³ and his colleagues at Mount Wilson Observatory, who used a chopping frequency of 1080 c.p.s. and an untuned pre-amplifier of voltage gain 300, followed by a tuned amplifier of voltage gain 10^5 .

Fig. 5.13 shows the resistance-coupled pre-amplifier. It consists of a 1620 (low-microphonic 6J7) pentode amplifier followed by a cathode-follower stage, the latter having an output impedance of 500 ohms. The values of circuit constants shown are those originally obtained from the publication, and some values had to be changed to suit the photo-cell being used.

The adopted photo-cell current was 150 microamps. and the measured resistance across the two sensitive elements in series was 500K, indicating a required D.C. potential across the photo-cell of 75 volts. The D.C. voltage at the high end of R_3 is given by $150R_2/(R_1+R_2)$. (R_1 and R_2 act as a voltage divider while R_2C acts as a decoupling filter). Since the photo-cell may be considered as a tube with plate resistance 0.5 M., it

3. E. B. Wilson & G. P. Kuiper - "Infra-red Spectra of Planets" *Astrophys. J.*, Vol. 106, p. 243, (1947).

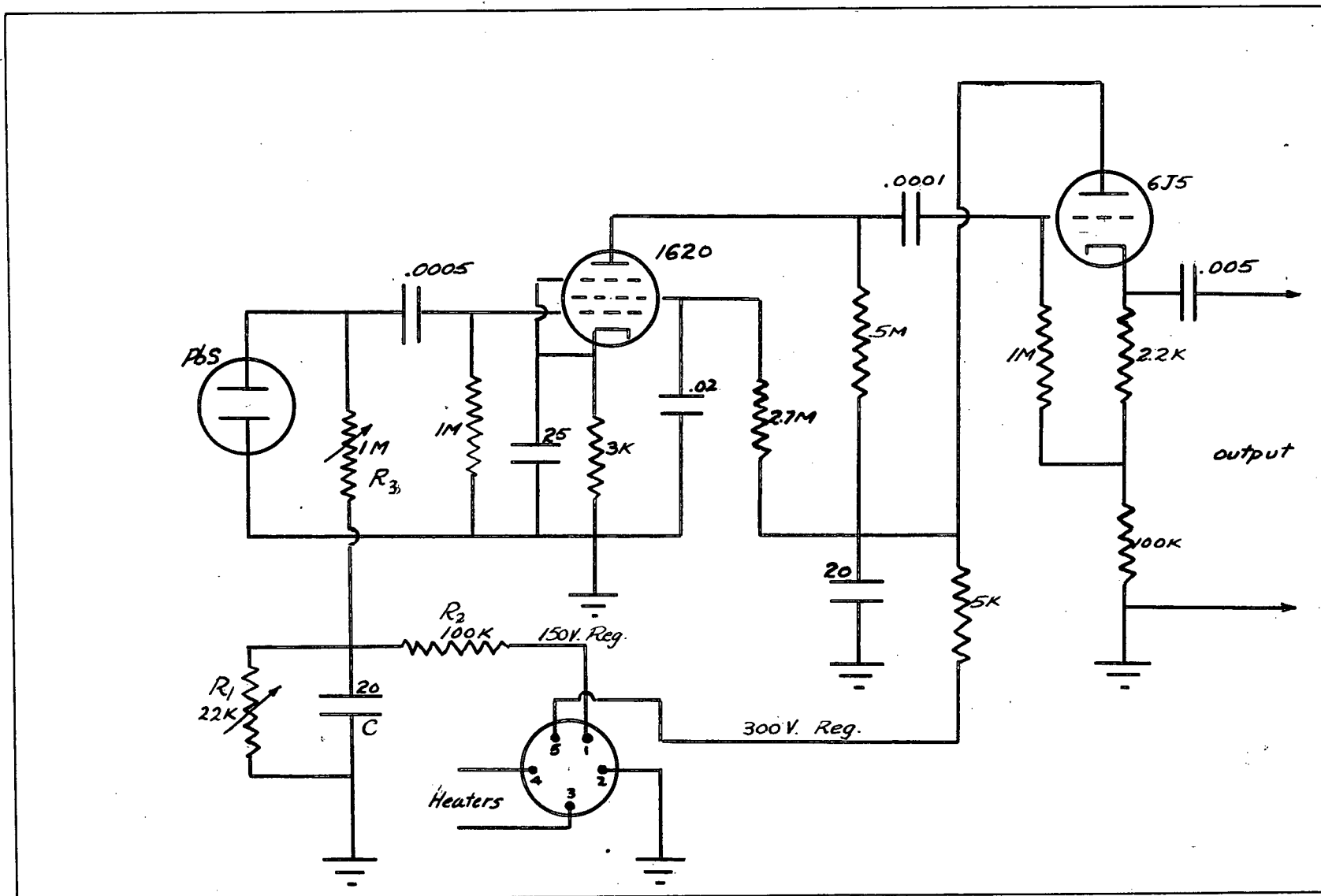


Fig. 5.13. Pre-amplifier

was desirable to keep R_3 at least equal to this value; which meant that the required D.C. voltage at R_3 was 150 volts and hence $R_1 = 0$. Apart from these changes, all other circuit constants are as shown. The cathode follower stage greatly simplified the problem of matching between pre-amplifier and amplifier.

E. THE MAIN AMPLIFIER AND POWER SUPPLY

The main amplifier is shown in Fig. 5.14. The gain control potentiometer feeds the signal onto the grid of a triode-connected 6SJ7, which has a gain of about 10 and is a buffer stage designed to isolate the gain control from the selective section. This ensures that the parallel resonant impedance of the tuned circuit is independent of the gain control setting.

The 2H inductance is formed from two toroidal coils in series, while the capacity branch consists of 0.0115 μ f and a 230 μ f padder condenser for fine tuning. This differs markedly from the original, which used a 22H inductance mounted in a two layer shield and a fixed capacity of 0.008 μ f. The advantage of the toroids is that they have no external field and hence pickup of extraneous signals is minimized. However, an added precaution was taken by mounting the inductance branch on a separate chassis and connecting it to the amplifier through a coaxial cable.

The amount of positive feedback, which effectively determines the Q of the L-C circuit, is controlled by potentiometer R_4 . Advancing the tap to the ground end increases the feedback. Tests taken with an audio amplifier input to the 1620 showed

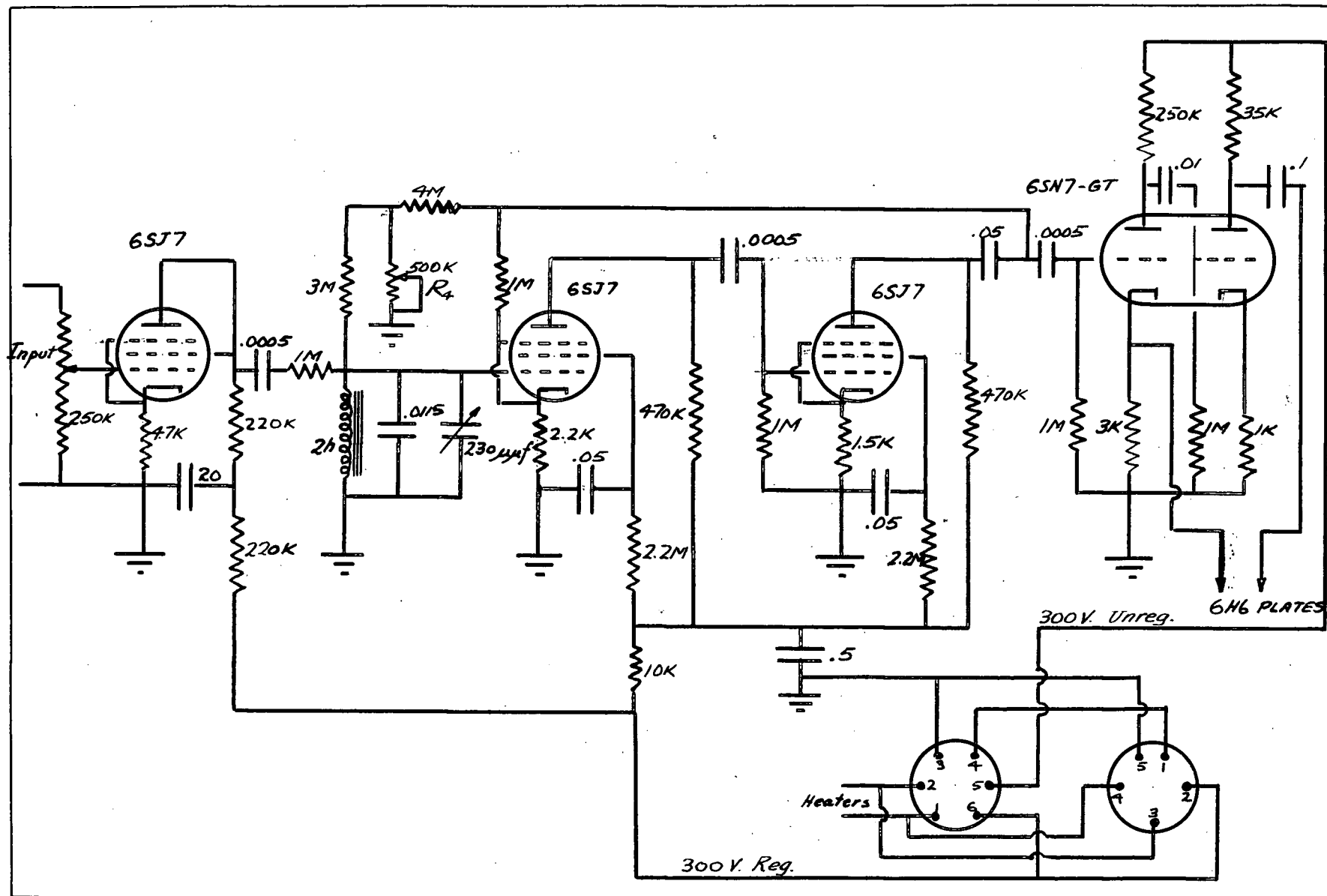


Fig. 5.14. Main amplifier

that a band width < 5 c.p.s. at 900 c.p.s. was possible with perfect stability.

The coupling and rectification circuits from the 6SN7-GT to the Brown Recorder are shown in Fig. 5.15. The return circuit from the second plate of ^{the} 6H6 going to ground through the 3K cathode resistor of the first triode section of the 6SN7-GT introduces 20 db. of negative feedback and effectively stabilizes the output. The 6H6 acts as a diode vacuum-tube voltmeter

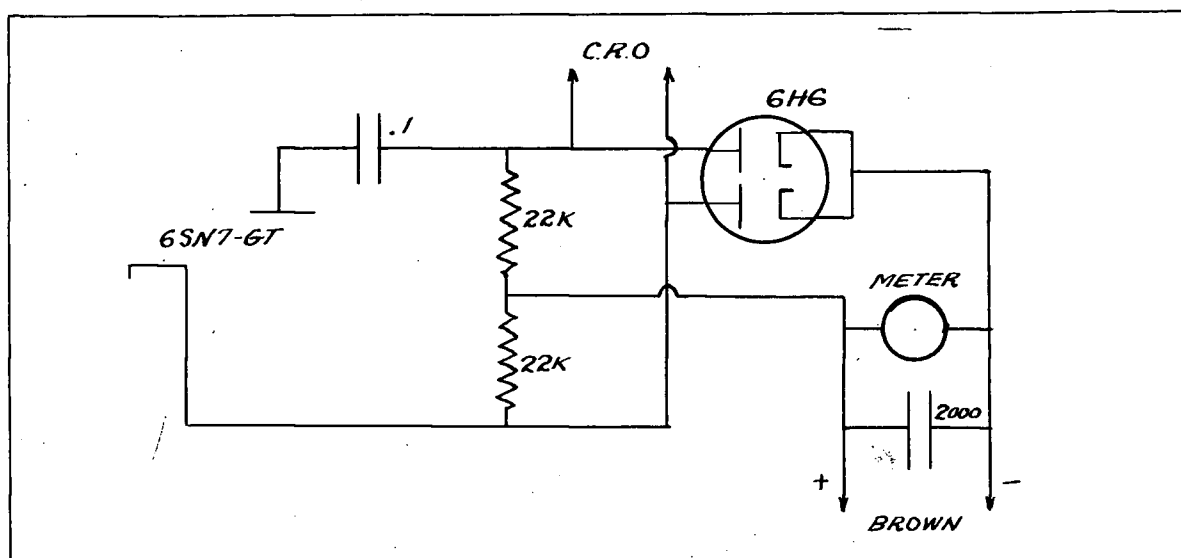


Fig. 5.15. Rectifier circuit for input to Brown Recorder.

and gives an output D.C. current up to 1 ma. (1 ma. for 2.5 V.A.C. input at the 6SN7-GT). The output saturates at 1.5 ma. and effectively protects the meter.

The potential across the input terminals of the Brown Recorder for a full scale deflection was found to be 10 millivolts. Further, the full scale deflection of the milliammeter (2 ma) was found to correspond to a potential of 80 millivolts, hence a signal that caused a full scale Recorder reading would be equivalent to a current of 0.25 ma. through the meter. This

provided a continual check of one reading against the other, besides which the meter functioned as a bleeder resistor across the Recorder input. The 2000 μ f condenser served to filter out all random signals of period less than 0.1 second, the time constant of the R-C network formed by the meter and the capacity.

The power supply is shown in Fig. 5.16. It has an ordinary two stage resistance-capacity filter, and voltage regulation is achieved by two VR-150 gaseous regulator tubes in series. With the exception of the 6SN7-GT, the plate supply voltage for all the tubes is regulated. The supply voltage for the photo-cell is taken from the second VR-150. A voltage divider consisting of 250K and 100K is connected from 150 volts regulated to ground, and the centre tap of the filament supply is connected to the top end of the 100K resistor. This raises the centre tap to a potential of 45 volts and makes both the grids and cathodes of the tubes very negative with respect to their filaments, and thus minimizes the leakage of 60 and 120 cycle signals into the amplifying circuits.

F. THE PERFORMANCE OF THE AMPLIFIER

The gain of amplifier and pre-amplifier were measured separately. A 900 c.p.s. input from an audio-oscillator was put into the amplifier and also onto the screen of a C.R.O. A fraction of the amplifier output was then put on the C.R.O. by a potentiometer so that the trace height was the same. The ratio of total resistance to the resistance from centre tap to ground then gave the gain directly. It was found that the total gain was 6×10^6 , about one fifth that claimed for the ori-

ginal. The difference may be accounted for by the lower parallel resonant impedance in the modified circuit due to the values of inductance and capacity differing from those originally published.

CHAPTER 6

FINAL ASSEMBLY

A. INTRODUCTION

In this chapter, a description is given of the various problems encountered in assembling the component parts of the spectrograph into the complete apparatus. It must not be supposed that all these problems occurred after the parts were constructed; indeed, there are features discussed here which had to be considered before any construction was begun. Therefore, the text of this chapter follows as closely as possible a chronological sequence.

B. OPTICS

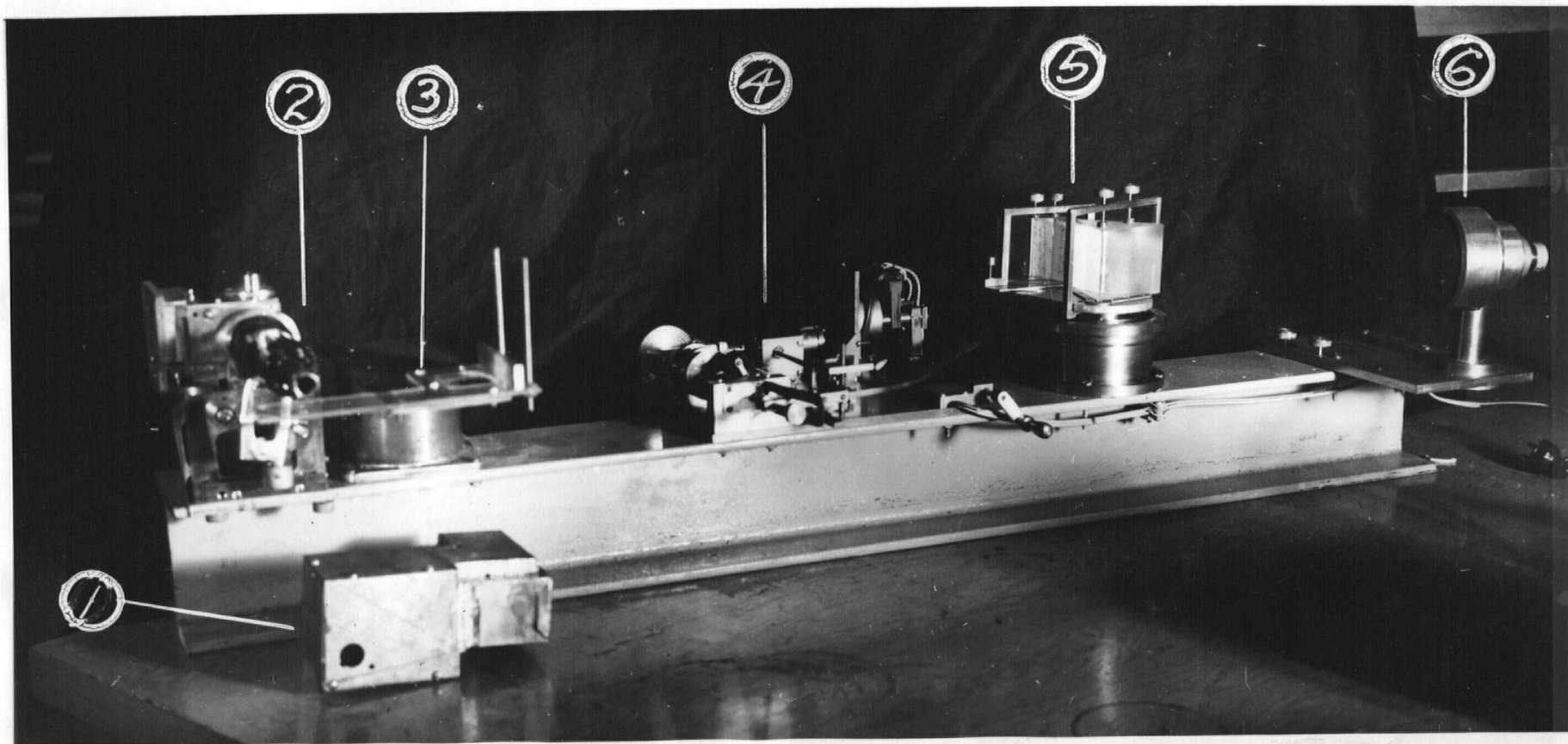
It was desirable to keep the overall length of the spectrograph to a minimum, so the off-axis paraboloid was placed at one end of the base beam and the slit unit at the other. Since slits, prisms, and mirror could not all be in a straight line, it was decided to offset the latter since it was virtually fixed in position once adjusted. It was also desirable to keep the width to a minimum, hence the mirror had to be as close to the axis of the beam as possible, but not so close as to allow the prism table to block any portion of the cone of rays from the entrance slit. This was essentially a graphical problem, and for design purposes was drawn full scale. The slit base was mounted on elongated holes to facilitate exact focussing.

The prism train was set up by protractor measurements

PLATE IV.

FRONT VIEW OF OPTICAL ASSEMBLY

1. Pre-amplifier (removed)
2. Slit unit
3. Pre-amplifier support
4. Scanning drive
5. Prism assembly
6. Parabolic mirror



since nothing was to be gained by more exact methods. Then, using a mercury arc, the prism table was rotated until the yellow doublet was at the exit slit and then locked. The micrometer was then set to some intermediate figure (temporarily) and the lever arm adjustment screw turned until the micrometer bore against its concave end. This adjustment can be seen in Plate 4. The prism train was fitted with an opaque dust cover, to block diffuse light that occurred at the slits due to full reflection from the front face of the half-prism.

Since no information could be obtained directly on the direction of the principle axis of the paraboloid, it had to be determined by rotating the mirror in its support until the line image was at maximum clarity.

C. ENCLOSING THE SPECTROGRAPH

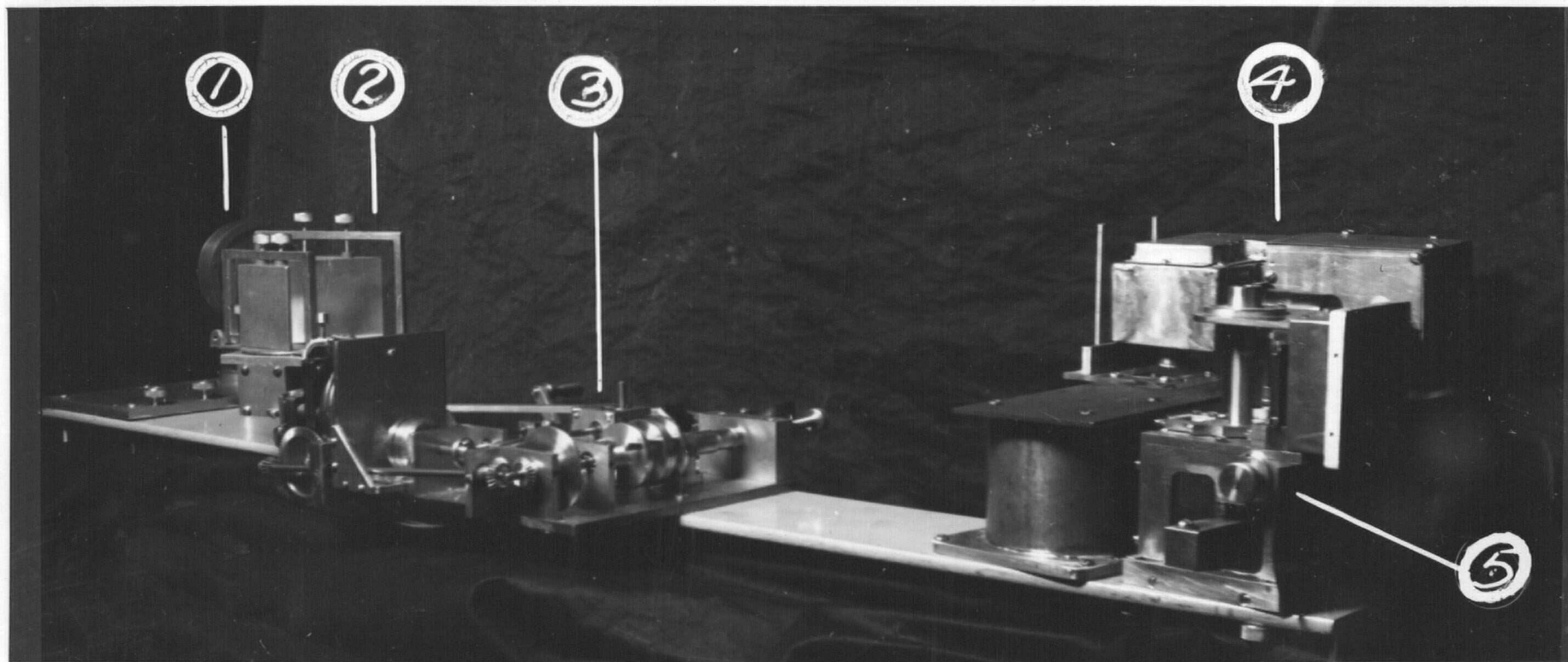
Upon the advice of Dr. Crooker, no attempt was made to put the optics in a vacuum. The spectrograph, photocell, and pre-amplifier were mounted in a wooden box blackened on the inside and provided with shutters at the front end for light-tightness. Originally, the bottom and sides of the box extended forward to support the chopping wheel, but the vibration proved to be excessive and finally the box was cut off parallel to the end of the base beam and the chopper mounted on a separate table. The final appearance can be seen in Plate 6. The twisted cable going into the box is the power supply for the pre-amplifier, while the coaxial cable to the main amplifier is directly behind.

The extension on the side of the box near the front was

PLATE V

REAR VIEW OF OPTICAL ASSEMBLY

1. Parabolic mirror
2. Prism assembly
3. Scanning drive
4. Pre-amplifier
5. Slit unit



necessary to accomodate the pre-amplifier, and the latter, on its support, was insulated from the spectrometer in order to avoid capacity effects. One difficulty encountered at this point was that of the photocell and pre-amplifier preventing the shutters from moving in and out freely, since the shutters were perpendicular to the beam axis while the slit assembly and photocell were inclined to it. This was overcome by making the exit slit parallel to the main beam, and it is shown in the revised position in Plate 3 (following page 32) and Plate 4.

The chopping wheel can be seen in Plate 6. The knurled wheel below the shaft moves the ball-bearing pillow blocks backwards or forwards and so adjusts the position of the chopping wheel while allowing the base to be fixed.

D. ELECTRONIC COMPONENTS

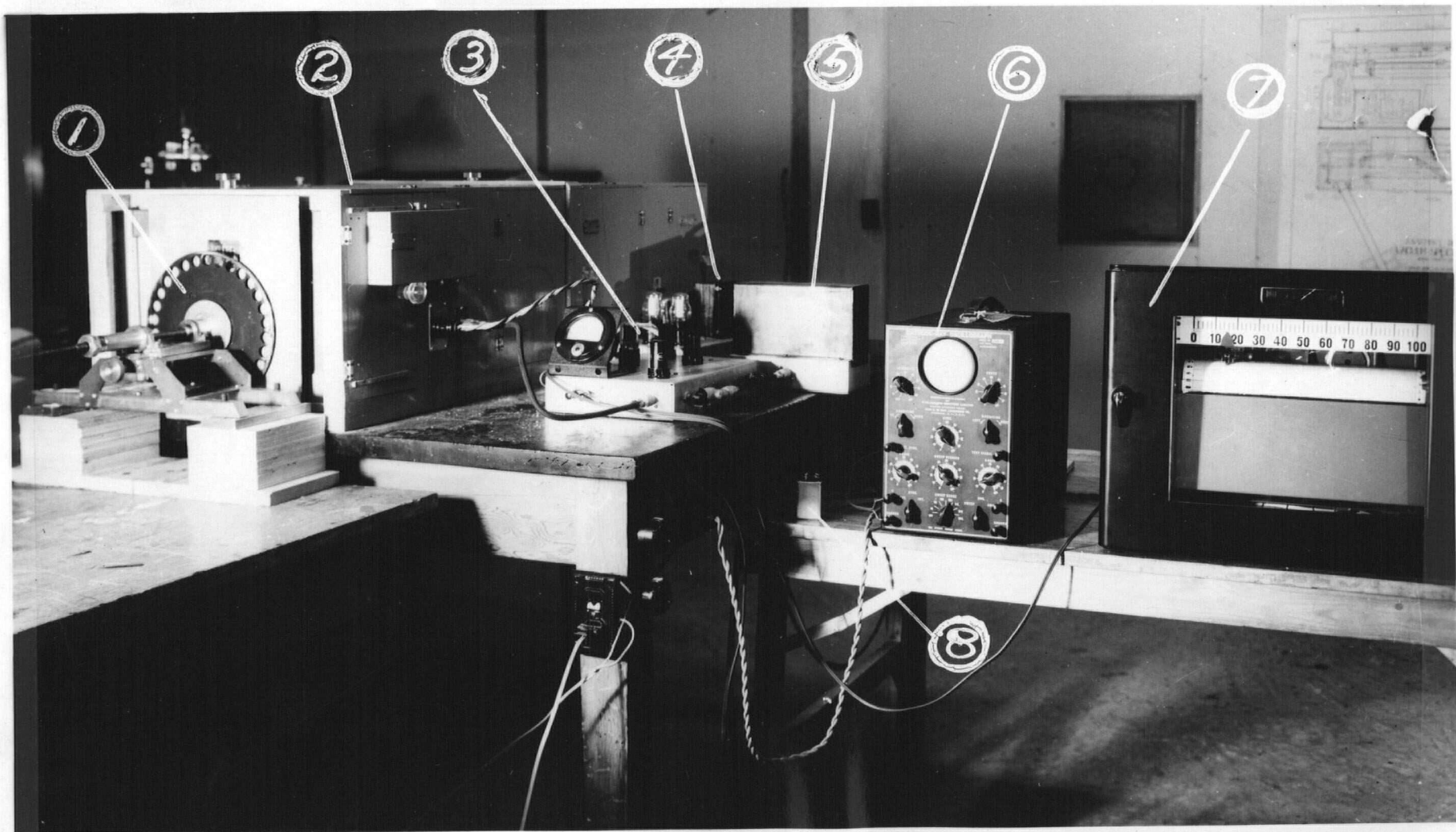
These are shown in Plate 6. The small transformer (8 in the figure) serves to isolate the ground of the C.R.O. from the cathode of the 6SN7-GT in the main amplifier. It was found that considerable "noise" was getting into the output because one side of the A.C. output of the amplifier was not grounded. No attempt was made to ground the Brown Recorder because the D.C. output of the amplifier was also floating.

The sensitized elements of the photoelectric cell were placed in optimum position in the emergent beam by slight adjustment of the annular ring supporting the front of the photocell. This was done with the mercury line at 5461 \AA on the exit slit. The socket for the photocell was allowed a little freedom of rotation in the pre-amplifier chassis so that the

PLATE VI

THE COMPLETE SPECTROGRAPH

1. Chopping wheel
2. Light-tight box
3. Main amplifier
4. Power supply
5. Inductance unit
6. Cathode-ray oscilloscope
7. Brown recording potentiometer
8. C.R.O. coupling transformer



sensitive elements could be made parallel to the exit slit. Their direction with respect to the base pins varied slightly from tube to tube. The on-off switch for the scanning drive was mounted on the outside of the box and can be seen in Plate 6 just above the power supply.

CHAPTER 7

RESULTS OF SPECTRA TAKEN
WITH THE SPECTROGRAPH: CONCLUSIONSA. INTRODUCTION

It was decided to use a mercury arc as a source of emission lines for the first tests of the instrument. There are several strong lines in the region 1μ to 2μ for which the wave numbers are known very accurately, and these were to be used as primary calibration points. Other fainter lines and groups of lines exist which were to serve as secondary calibration points and, in some cases, as criteria for resolving power and sensitivity.

B. EXPERIMENTAL

The final result of much research into the problem of obtaining a good spectrum is shown in Plate 7, and was only obtainable after many runs had been made with different combinations of slit width, photocell orientation, and amplifier settings. The author believes that Plate 7 represents the best possible results obtainable on this instrument with the mercury arc.

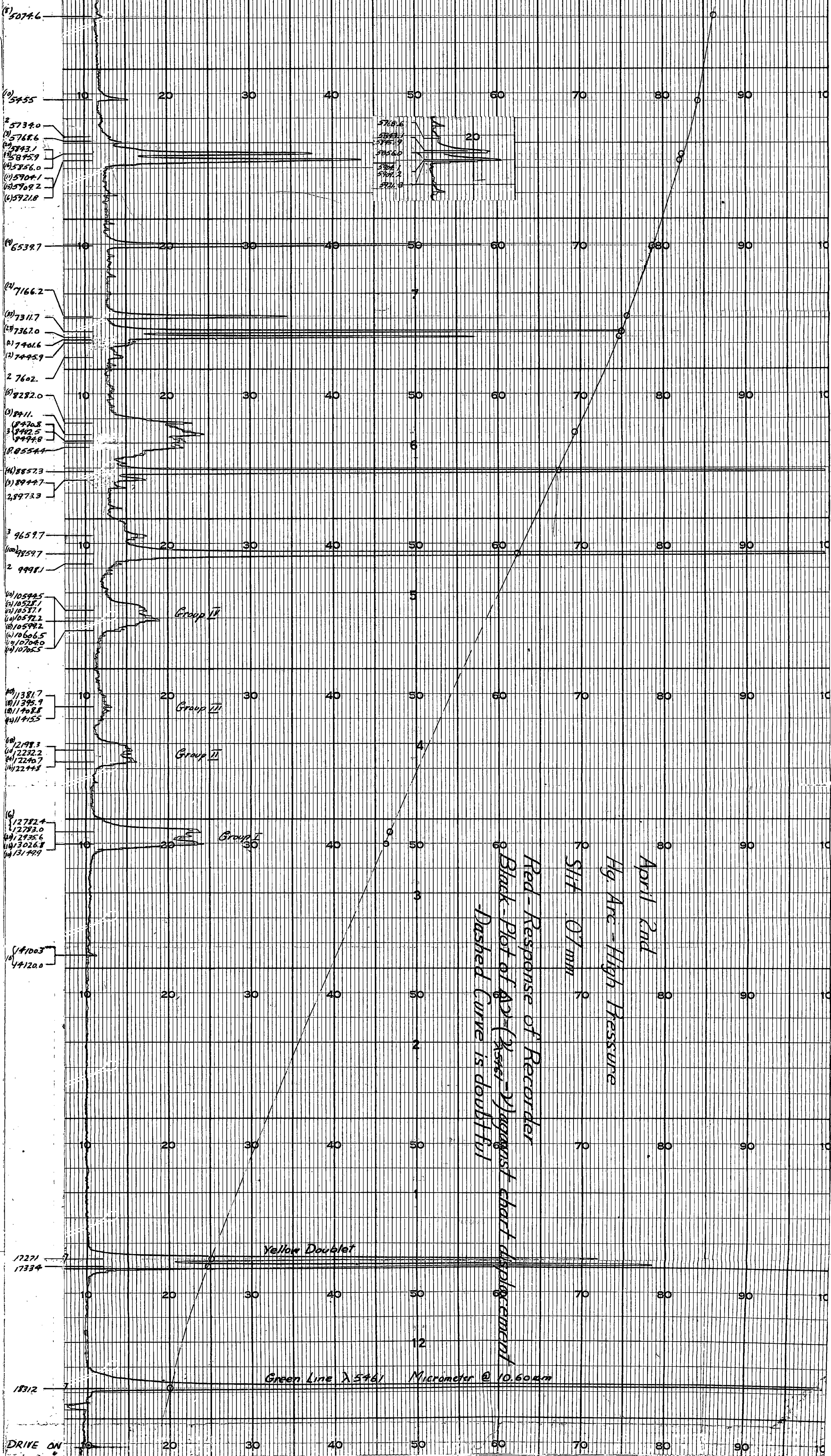
As can be seen, the cut-off limit appears to be about 2μ . However, later investigation of continuous sources (e.g. the carbon arc) indicated that the optics of the spectrograph were transmissive up to about 2.3μ , which indicates that the termination of the spectrum was due to the double glass envelope of

PLATE VII

SPECTRUM OF Hg I

TAKEN WITH THE SPECTROGRAPH

Bracketed
Intensities
are predicted
from previous
data
I V



the arc itself. In fact, the prism table lever arm was adjusted so that the cut-off switch would allow the spectrum to be covered out to 2.3μ . Scanning was commenced just before the green line at 5461 \AA , this being an excellent datum wave length from which to work.

Plate 7 represents one copy of three similar spectra which were taken successively on the noted date. These runs were taken in the evening, because it was found that the switching on and off of electrical circuits in the vicinity caused small pulses to appear on the chart. As a first approximation to drawing some kind of dispersion curve, the wave lengths of the prominent lines were taken from a handbook of physics⁴, and the wave number interval between the line in question and the green line was plotted on a vertical scale directly on the chart. It can be seen that the dispersive properties of the optical system differed markedly from those predicted, since the expected crowding at long wave lengths does not occur and the dispersion on a wave number scale is nearly linear.

To identify some of the less prominent lines, it was first necessary to obtain more exact wave numbers for the primary standards and the author is indebted to Dr. A. M. Crooker for the term table which was used for this. Several other references were consulted⁵ to find the theoretical and experimental relative intensities of lines, and in general the values in () in Table 7.8 are averaged from several sets of data and from considerations of the transitions involved. The adopted primary wave number values are marked with a (†).

4,5. See bibliography.

Table 7.8. Mercury I.

Wave numbers and transitions of lines.
 $\nu = 5,000$ to $\nu = 10,000$ cm^{-1} .

(*) - appear on chart (Plate 7)

(†) - primary standards

(I) - assumed relative intensities (scale 1-100)

I - measured or predicted intensities (scale 1-100)

x = $5d^9 6s^2 6p$

ν	Transition	I	ν	Transition	I
* 9998.1	$6s7p^3P_1 - 6s8d^1D_2$	2	* 8494.8	$6s7p^3P_2 - 6s8d^3D_3$	4
*† 9859.7	$6s6p^1P_1 - 6s7s^1S_0$	(100)	* 8482.5	$6s7p^3P_2 - 6s8d^3D_2$	2
* 9659.7	$x^3P_0 - 6s7d^3D_1$	3	* 8470.8	$6s7p^3P_2 - 6s8d^3D_1$	0
9329.8	$x^3P_2 - 6s9s^3S_1$	1	8452.5	$6s7p^3P_2 - 6s8d^1D_2$	0
9243.4	$x^3P_1 - 6s7d^3D_2$	0	8414.3	$6s6d^1D_2 - 6s6f^3F$	0
9220.1	$x^3P_1 - 6s7d^3D_1$	0	* 8409.9	$6s6d^3D_1 - 6s6f^3F_2$	(3)
9199.1	$x^3P_1 - 6s7d^1D_2$	0	8410.6	$6s6d^1D_2 - 6s6f^1F_3$	0
9070.1	$6s7p^1P_1 - 6s10s^1S_0$	2	8395.1	$6s7p^1P_1 - 6s8d^3D_2$	0
9060.7	$6s7p^3P_2 - 6s10s^3S_1$	1	8383.4	$6s7p^1P_1 - 6s8d^3D_1$	0
* 8973.3	$6s7p^1P_1 - 6s7s^3S_1$	2	8365.1	$6s7p^1P_1 - 6s8d^1D_2$	(1)
* 8944.7	$6s7s^3S_1 - 6s7p^1P_1$	(3)	8352.2	$6s6d^3D_2 - 6s6f^3F_3$	(2)
*† 8857.3	$6s7s^3S_1 - 6s7p^3P_2$	(46)	8347.3	$6s6d^3D_2 - 6s6f^1F_3$	0
8741.7	$6s7p^3P_1 - 6s9s^1S_0$	0	8315.2	$6s6d^3D_3 - 6s6f^3F_4$	(2)
8699.9	$6s7p^3P_0 - 6s9s^3S_1$	0	8301.3	$6s6d^3D_3 - 6s6f^1F_3$	0
* 8554.4	$6s7p^3P_1 - 6s9s^3S_1$	(1)	* 8282.0	$6s6p^1P_1 - 6s7s^3S_1$	(5)

Table 7.8. - Continued.

ν	Transition	I	ν	Transition	I
8242.8	$x^3P_2-6s7d^3D_3$	(2)	5906.4	$6s6d^1D_2-6s5f^3F_3$	4
8221.3	$x^3P_2-6s7d^3D_2$	1	5904.1	$6s6d^1D_2-6s5f^3F_2$	(11)
8198.0	$x^3P_2-6s7d^3D_1$	0	5900.9	$6s7p^3P_2-6s7d^3D_2$	(10)
8177.0	$x^3P_2-6s7d^1D_2$	0	*† 5856.0	$6s7p^3P_2-6s7d^1D_2$	(16)
7568.1	$6s7p^3P_0-6s7d^3D_1$	(2)	*† 5845.9	$6s6d^3D_2-6s5f^1F_3$	(13)
7480.1	$6s6d^1P_2-6s8p^1P_1$	5	* 5843.1	$6s6d^3D_2-6s5f^3F_3$	(20)
7476.9	$6s8p^3P_0-6s6d^3D_1$	0	5840.8	$6s6d^3D_2-6s5f^3F_2$	5
* 7445.9	$6s7p^3P_1-6s7d^3D_2$	(2)	5812.9	$6s7p^1P_1-6s7d^3D_2$	0
7422.6	$6s7p^3P_1-6s7d^3D_1$	0	5811.8	$6s6d^3D_3-6s5f^3F_4$	(2)
7416.8	$6s6d^3D_1-6s8p^1P_1$	(1)	5809.9	$6s6d^3D_3-6s5f^1F_3$	0
* 7401.6	$6s7p^3P_1-6s6d^1D_2$	(2)	5807.1	$6s6d^3D_3-6s5f^3F_3$	(3)
*† 7367.0	$6s7s^1S_0-6s7p^1P_1$	(23)	5804.8	$6s6d^3D_3-6s5f^3F_2$	0
*† 7311.7	$6s7s^3S_1-6s7p^3P_1$	(33)	5789.6	$6s7p^1P_1-6s7d^3D_1$	0
*† 7166.2	$6s7s^3S_1-6s7p^3P_0$	(12)	* 5768.6	$6s6p^1P_1-6s7d^1D_2$	(3)
7108.7	$6s7p^1P_1-6s9s^1S_0$	5	* 5734.0	$6s7s^1S_0-6s7p^3P_1$	1
7008.8	$6s7p^3P_2-6s9s^3S_1$	1	5490.4	$6s6d^1D_2-6s8p^3P_2$	0
*† 6539.7	$x^3P_1-6s8s^1S_0$	(19)	5487.3	$6s6d^1D_2-6s8p^3P_2$	0
6096.7	$x^3P_1-6s8s^3S_1$	1	5427.2	$6s6d^3D_2-6s8p^3P_2$	2
*† 5921.8	$6s7p^3P_2-6s7d^3D_3$	(5)	5391.2	$6s6d^3D_3-6s8p^3P_2$	10
*† 5909.2	$6s7d^1D_2-6s5f^1F_3$	(15)	*† 5074.6	$6s7s^3S_1-x^3P_0$	(10)

No signal on the chart was identified as a line unless it appeared on four runs. The approximate wave numbers of secondary lines were calculated by measuring the dispersion (on a

scale) between two primary lines on either side of the line in question and interpolating linearly for the desired wave number. This was first done for $\nu < 10,000 \text{ cm}^{-1}$, and after all lines had been measured, a successful attempt was made to correlate these values with the expected wave numbers from certain transitions. The measured value was usually within 5 wave numbers of that predicted.

A paper by McAlister⁶ was found useful. He used a vacuum thermocouple and thus was able to obtain a very good relative intensity scale. Since that paper was written, several lines then unaccounted for have been verified (notably transitions from $5d^9 6s^2 6p^3 P_{0,1,2}$) and also it appears that he incorrectly identified others. The wave numbers in Table 7.8 are taken from the term table and those lines which have been identified on the chart are marked with a (*). Of special interest is a portion of a spectrum, taken with a very narrow slit, appended to Plate 7 showing the complex line structure between $\nu = 5912.8$ and 5843.1 cm^{-1} . The line height on the chart is not proportional to the relative intensity except for a small interval, since the sensitivity of the photocell is not constant with wave length.

The identification of individual lines between 0.7μ and 1μ was difficult, and it was only possible to identify groups as shown on the chart. The wave numbers and intensities of all but the faintest lines were obtained from Weidmann and Schmidt⁷ and then corrected by identifying the lines in the term table.

6, 7. See bibliography.

These are listed in Table 7.9.

As a matter of interest, it was decided to identify the components of the groups 6smfF-6s6d^{1,3}D_{1,2,3} more exactly than had been done in the above paper, and for this purpose the author extended Dr. Crooker's term table to odd terms, as far out

Table 7.9. Mercury I.

Wave numbers and transitions of lines 0.7 μ to 1 μ .

All configurations except (x) include a 6s electron. F levels for a given m are not distinguished for m \geq 8.					
ν	Transition	I	ν	Transition	I
9998.1	7p ³ P ₁ - 8d ¹ D ₂	3	10751.8	7p ³ P ₀ -10s ³ S ₁	4
10016.2	7p ³ P ₁ - 8d ³ D ₁	4	10773.5	x ³ P ₂ - 8d ¹ D ₂	2
10028.1	7p ³ P ₁ - 8d ³ D ₂	6	10791.8	x ³ P ₂ - 8d ¹ D ₂	2
10052.5		4	10803.5	x ³ P ₂ - 8d ³ D ₂	4
10161.9	7p ³ P ₀ - 8d ³ D ₁	6	10815.8	x ³ P ₂ - 8d ³ D ₃	8
10208.5	7p ³ P ₂ -11s ³ S ₁	2	$\left. \begin{array}{l} 11059.1 \\ 11119.0 \\ 11122.4 \end{array} \right\} \begin{array}{l} 7d \\ 8d \end{array}$	9f F - 6d ³ D ₂	3
10527.9	8f F - 6d ¹ D ₂	2		9f F - 6d ³ D ₁	3
10527.9	8f F _p - 6d ¹ D ₂	6		9f F - 6d ¹ D ₂	3
10588.0	8f F - 6d ³ D ₁	6		7p ¹ P ₁ -11d ¹ D ₂	3
10591.2	8f F _q - 6d ¹ D ₂	5	11241.6		4
10594.0	8f F _r - 6d ¹ D ₂	5	11381.7	x ³ P ₂ -10s ³ S ₁	5
10597.7	7p ¹ P ₁ -10d ¹ D ₂	4	11395.0	7p ³ P ₁ - 9d ¹ D ₂	4
10606.3	7p ³ P ₁ -10s ³ S ₁	3	11408.9	7p ³ P ₁ - 9d ³ D ₁	4
10704.0	7p ³ P ₂ -10d ³ D ₃	5	11414.6	7p ³ P ₁ - 9d ³ D ₂	6
10705.5	7p ³ P ₁ -10s ¹ S ₀	5	11482.3	10f F - 6d ³ D ₁	3

Table 7.9. - Continued.

ν	Transition	I	ν	Transition	I
11485.5	10f F - 6d ¹ D ₂	4	12935.6		10
11509.7	7p ¹ P ₁ -12d ¹ D ₂	3	13021.4	Group I	2
11608.5		3	13025.0		8
11649.3	11f F - 6d ³ D ₃	3	13149.1		5
11683.9	11f F - 6d ³ D ₂	3	13253.5		3
11754.1	7p ³ P ₁ -11s ³ S ₁	5	13294.6	7p ³ P ₀ -12d ³ D ₁	3
11899.6	7p ³ P ₀ -11s ³ S ₁	3	13411.8	7p ³ P ₁ -13d ³ D ₁	3
12170.4	x ³ P ₂ -9d ¹ D ₂	1	13560.0	x ³ P ₂ -11d ³ D ₃	5
12184.3	x ³ P ₂ -9d ³ D ₁	0	13704.2	x ³ P ₂ -13s ³ S ₁	4
12190.6	x ³ P ₂ -9d ³ D ₂	4	13751.8	7p ³ P ₀ -14d ³ D ₁	3
12198.2	x ³ P ₂ -9d ³ D ₃	9	13928.1	x ³ P ₂ -12d ³ D ₃	4
12230.7	7p ³ P ₁ -10d ¹ D ₂	5	14028.2	x ³ P ₁ -10d ¹ D ₂	3
12239.7	7p ³ P ₁ -10d ³ D ₁	7			
12246.0	7p ³ P ₁ -10d ³ D ₂	8			
12385.2	7p ³ P ₀ -10d ³ D ₁	5			
12461.6	7p ³ P ₁ -11s ³ S ₁	3			
12529.5	x ³ P ₂ -11s ³ S ₁	4			
12607.1	x ³ P ₂ -12s ³ S ₁	3			
12779.7	7p ³ P ₂ -11d ³ D ₁	3			
12783.0		10			

as 6s12f F. The energy levels out to 6s6f^{1,3}F_{2,3,4} were obtained from Bacher and Goudsmit⁸, but subsequent values had to be

8. See Bibliography.

obtained by getting approximate solutions of the Rydberg formula and determining the approximate wave numbers of the expected transitions. By a consideration of probable relative intensities of lines, it was possible to identify certain lines in the table and thence obtain the correct (average) values of the energy levels. Those lines expected to be fairly strong (singlet-singlet, J and L changing in the same sense, and high-J transitions) were readily identified, and agreed with Weidmann and Schmidt's intensities, thus indicating the validity of the identification.

The identification of groups on the spectrum was carried out by looking for portions of the table containing stronger-than-average lines and seeing if they would approximately fit the dispersion curve. The final grouping is noted on the spectrum, and the author found that other papers⁵ with a photographic spectrum of the region were useful in the assignment of values. The agreement is quite good except that group I should be about twice as wide if the adopted intensities are correct.

C. CONCLUSIONS

From the wave numbers of lines resolved in the sectional spectrum appended to the main chart, the resolving power is seen to be at least 1,000 at 1.7μ , which compares favourably with the calculated value of 500. This is to be expected since the dispersion curve approximates a $\frac{1}{\lambda}$ variation instead of $\frac{1}{\lambda^2}$. The line at $\nu = 5455\text{cm}^{-1}$ is obtained from the handbook⁴ but cannot be found among the allowed transitions in the term table;

which indicates that either the dispersion curve is completely erroneous (which is doubtful) or that the line is due to a forbidden transition. The line at $\nu = 7602.5 \text{ cm}^{-1} \pm 2.5 \text{ cm}^{-1}$ definitely exists and also cannot be found.

Several strong lines between 0.7 and 1μ cannot be identified on the term table. According to the M.I.T. wavelength tables, there are lines due to Hg II at $\nu = 10054 \text{ cm}^{-1}$, (investigated by Rasmussen) Hg I at $\nu = 10055, 11243, 11609, 11785$, and 12939 cm^{-1} , (investigated by Suga, Kamyana, and Sugura at Tokyo) and Hg I at $\nu = 12786 \text{ cm}^{-1}$. (Scientific papers of the Tokyo Institute of Physics and Chemistry). None of these publications were available to the author. Exact details of the references may be found in the M.I.T. wave length tables (1939).

Attempts were made to obtain more precise data on the region 0.7 to 1μ by the use of continuous sources and absorption spectra. However, it was found that all sources using alternating current had 120 cycle intensity fluctuations that heterodyned with the chopping wheel. This was true of the carbon arc and the Nernst glower. On the other hand, the D.C. power supply was too unsteady for efficient operation of the Nernst, and the proper D.C. carbons for the arc were not obtainable.

The performance of the spectrograph thus far indicates that, while not as convenient to use as the Perkin-Elmer instrument, it has a much better resolving power in the region thus far worked. The author hopes to further investigate its performance, and regrets that results obtained will not be complete in time for inclusion in this paper.

It can be concluded that the PbS photoelectric cell is, in spite of its non-linearity, at least the equal in performance of any other detector in the near ($<3\mu$) infra-red.

BIBLIOGRAPHY

A. References referred to in the foot-notes, in the order of appearance

1. Thiene, H., Glas, Jena, Gustave Fischer, 1931.
2. Czapski, S., and Eppenstein, O., Grundzüge der Theorie der Optischen Instrumente, Leipzig, Johann Barth, 1924.

A detailed study of the geometrical optics of the slit curvature problem leads to the general formula:

$$r = \frac{fn \sqrt{1 - n^2 \sin^2 \left(\frac{A}{2} \right)}}{2(n^2 - 1) \sin \left(\frac{A}{2} \right)}$$

where A is the prism angle.

When $A = 60^\circ$, as in this paper, formula 4.1 is the result.

3. Wilson, E.B., and Kuiper, G.P., "Infra-red Spectra of Planets," Astrophysical Journal, vol. 106, p.243, (1947).

Their photocell was also dry-ice cooled, but the sensitivity increase was not sufficient to justify the time involved in preparation. The author of the present paper found that the entire volume of solid CO_2 sublimed before the runs were half completed.

- 4,5. Handbook of Chemistry and Physics, Cleveland, Chemical Rubber Publishing Co., 1949, pp. 2180 and 2248.

The source for the approximate wave numbers of primary standards. The line at $\nu = 5455 \text{ cm}^{-1}$, which cannot be identified with a transition, is listed here.

5. Kayser, H., Handbuch der Spektroskopie, VII, 2, Leipzig, S. Hirzel, 1901, p. 669.

Gives the wave lengths of lines due to Hg I from 40159 Å to 8195.6 Å. The agreement with Schmidt and Weidmann (7) is good above 10,000 Å but poor otherwise.

x

BIBLIOGRAPHY - continued

5. McLennan, J.C., Smith, H.D., and Peters, R., "Wave Lengths in the Infra-Red Spectrum of Mercury," Transactions of the Royal Society of Canada, Section III, vol. 19, p. 39, (1925).

The transitions and wave numbers are not very accurate. The photographs of infra-red spectra were useful in locating groups of lines in Plate 7.

- 5,6. McAlister, E.D., "The Spectrum of the Neutral Mercury Atom in the Wave Length Range from 1 to 2 μ ," Physical Review, vol. 34, p. 1142, (1929).

An excellent reference for relative intensities of lines, generally adopted in the present paper. The wave numbers are not in very good agreement with later values.

7. Schmidt, W., and Wiedmann, G., "Über das Bogenspectrum des Quecksilbers im Infrarot," Zeitschrift für Physik, vol. 106, p. 273, (1937).

Gives λ and ν of lines from 7097 Å to 12,156 Å. The agreement with the term table is good. The given relative intensities and reproductions of photographic spectra were useful in identification of groups between 7000 Å and 10,000 Å.

8. Bacher, R.F., and Goudsmit, S., Atomic Energy States, New York, McGraw-Hill, 1932, p. 227.

The reference consulted for the term values of $6s m f^{1,3} F_{2,3,4}$ states. Assuming the validity of

$$T = \frac{R}{(n - \alpha + \beta/n^2)^2}$$

and the term values given, one finds the following relation between calculated and experimental values of the levels $6s m f F$: (After $m = 8$, the observations do not indicate an appreciable difference between the levels for a given m).

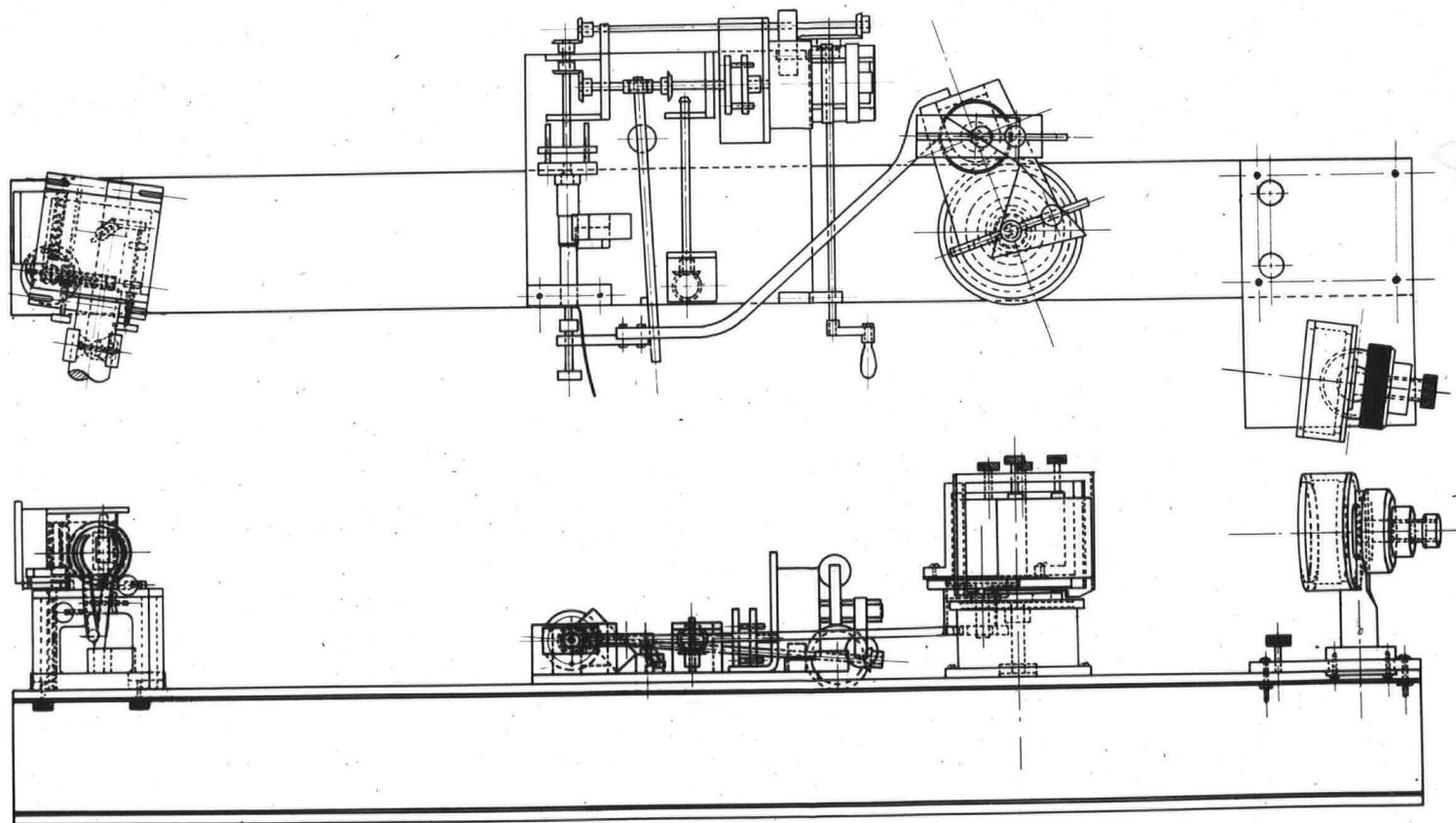
~~21~~

BIBLIOGRAPHY - continued

m	$3F_{4,3}$		$3F_2$		$1F_3$	
	Calc.	Obs.	Calc.	Obs.	Calc.	Obs.
7	3072.9	3073.9	3075.9	3077.0	3081.2	3077.0
8	2255.2	2257.1	2256.9	2257.1	2260.2	2257.1
9	1725.2	1725.9	1726.3	1725.9	1728.5	1725.9
10	1362.2	1362.8	1363.0	1362.8	1364.5	1362.8
11	1102.8	1101.4	1103.3	1101.4	1104.4	1101.4
12	911.0	908.8	911.4	908.8	912.2	908.8

B. General references

1. Harrison, G.R., Lord, H.C., and Loofbourow, J.R., Practical Spectroscopy, New York, Prentice-Hall, 1948.
2. M.I.T. Wavelength Tables, New York, John Wiley and Sons, 1939.
3. Sawyer, R.A., Experimental Spectroscopy, New York, Prentice-Hall, 1944.

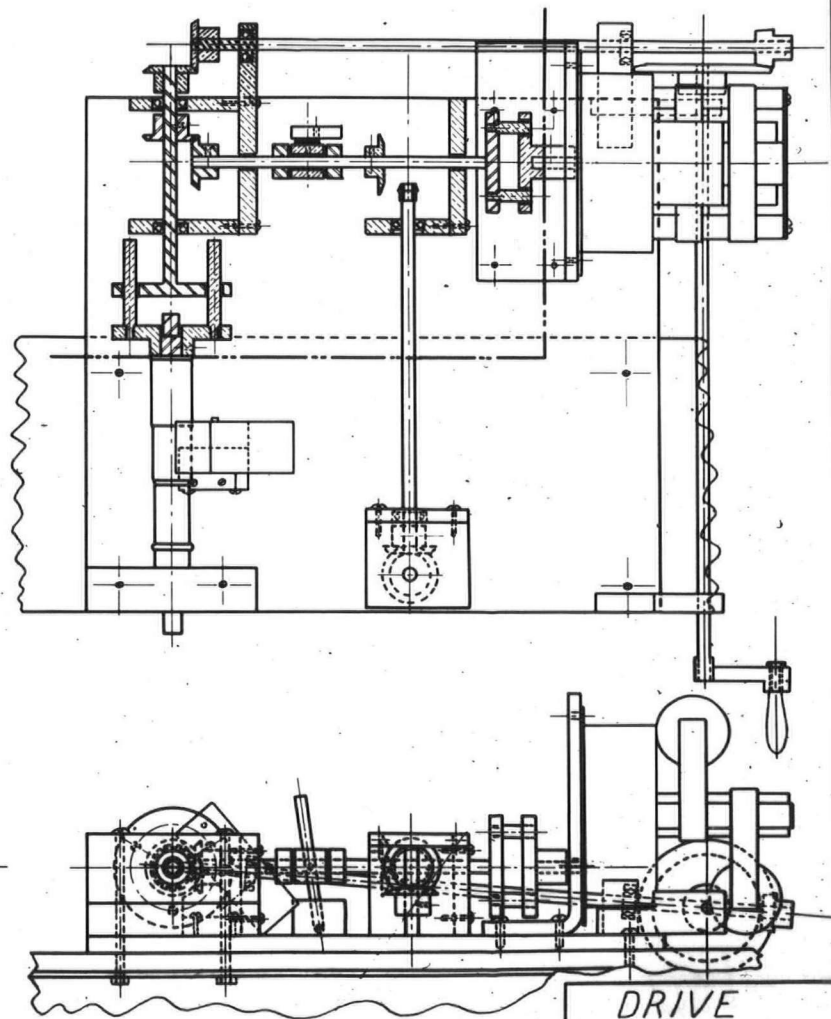
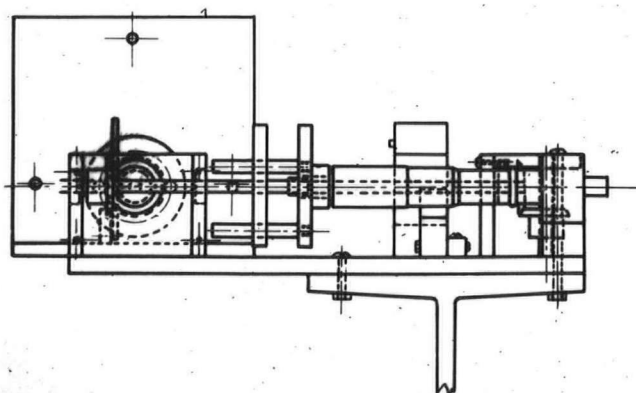


ASSEMBLY OF THE
INFRA-RED
SPECTROGRAPH

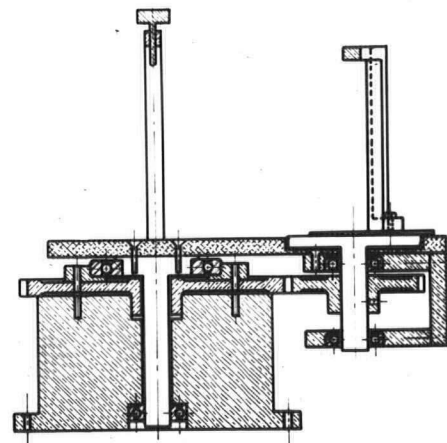
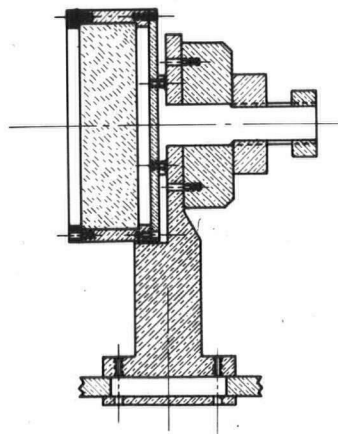
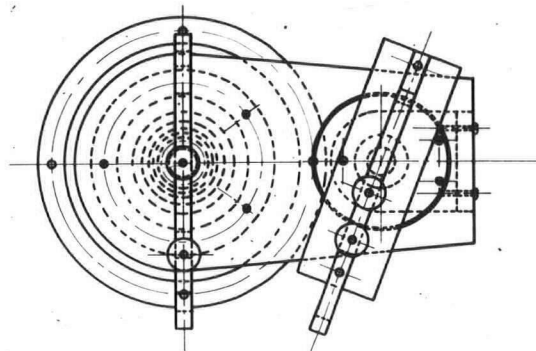
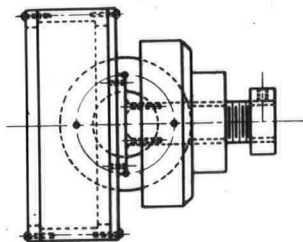
PHYSICS, UBC
Scale: $\frac{1}{2}$ Size
Drawn By *offhandy*

1

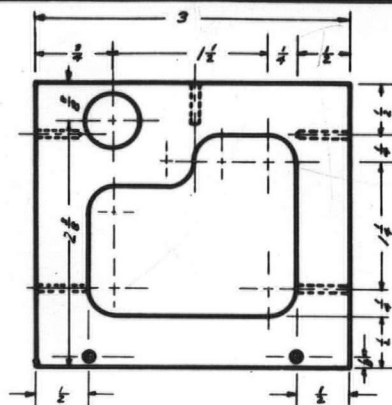
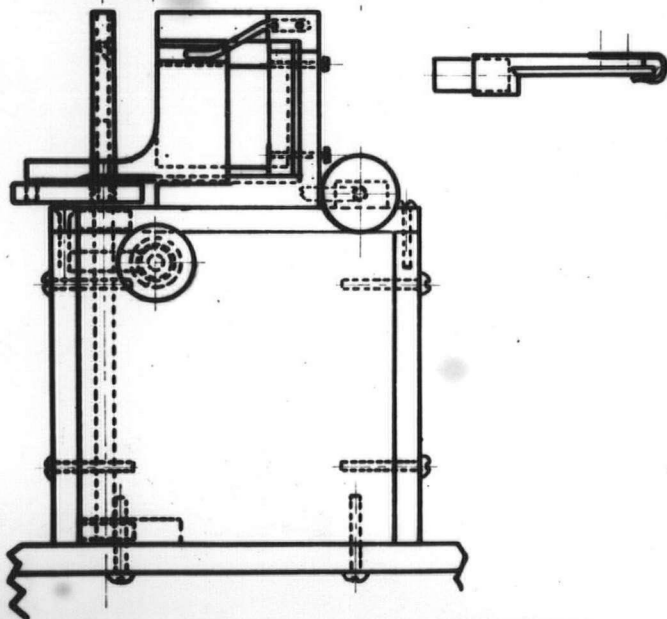
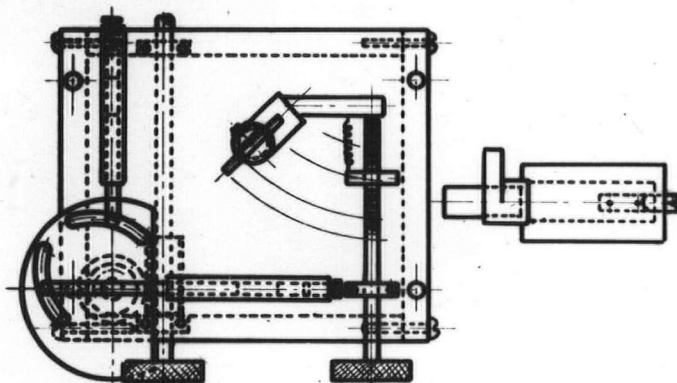
See Next Dwg. for Linkage of Drive to Table and Slit



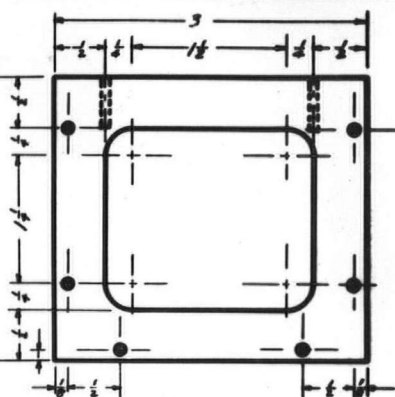
DRIVE
for
PRISM TABLE
PHYSICS DEPT., U.B.C.
Drawn By *W. J. B.*
Date *1/1/30* Sheet No. 2



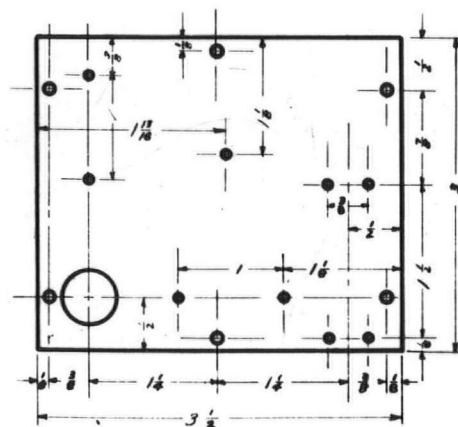
ASSEMBLIES OF
PRISM TABLE
MIRROR CELL
PHYSICS, UBC
Scale - Full Size
Drawn By *GRB/ushy* 3



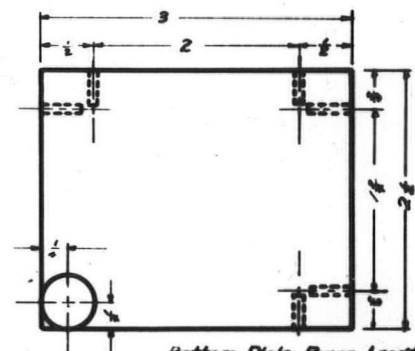
Front Plate Brass 2 regd.



Side Plate Brass 2 regd.



Top Plate Brass 1 regd.

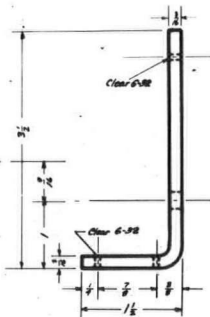
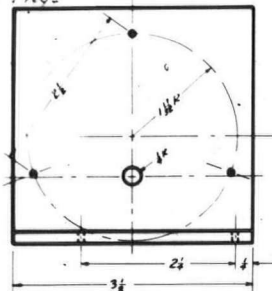


Bottom Plate Brass 1 regd.

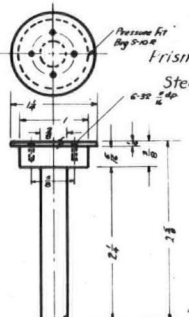
All tapped holes - 6-32 ~ 1/2 Deep

SPECTROGRAPH
SLIT
ASSEMBLY & BASE MOUNT
PHYSICS DEPT. U.B.C.

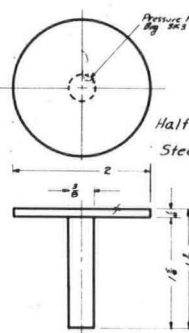
Motor Mount
Brass, 1 reqd



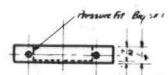
Prism Table Pivot
Steel, 1 reqd.



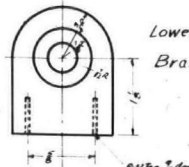
Half-Prism Table
Steel, 1 reqd.



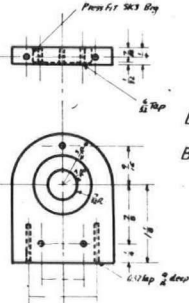
Pressure Fit
By 3-11



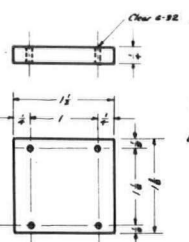
Lower Yoke
Brass, 1 reqd



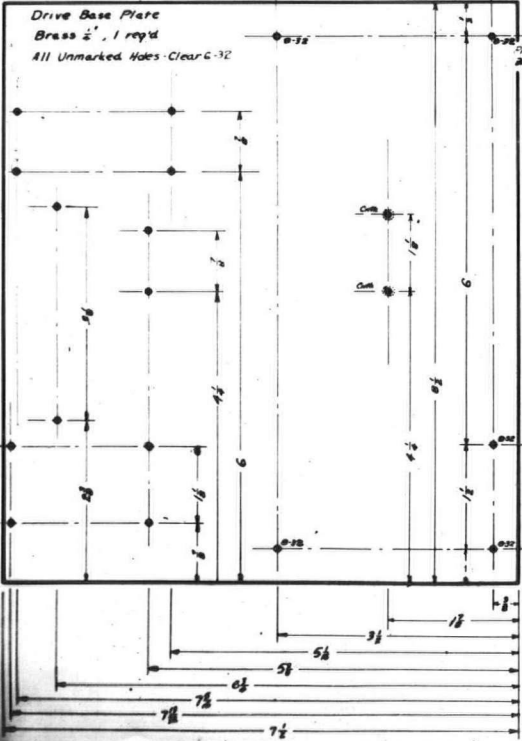
Lower Yoke
Brass, 1 reqd



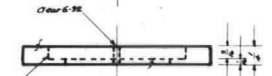
Yoke Link
Brass, 1 reqd



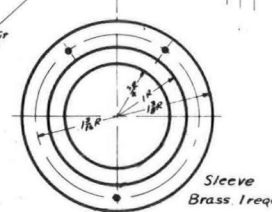
Drive Base Plate
Brass 1/2", 1 reqd
All Unmarked Holes Clear 6-32



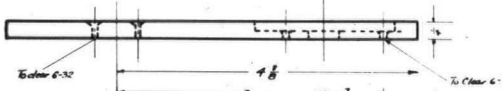
Clear 6-32



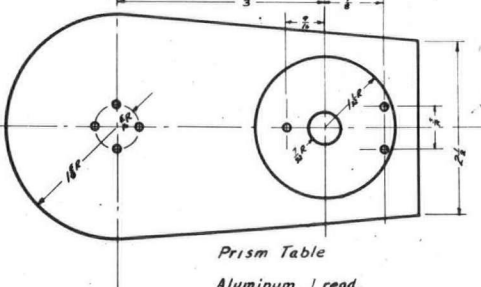
Sleeve
Brass 1 reqd



Clear 6-32

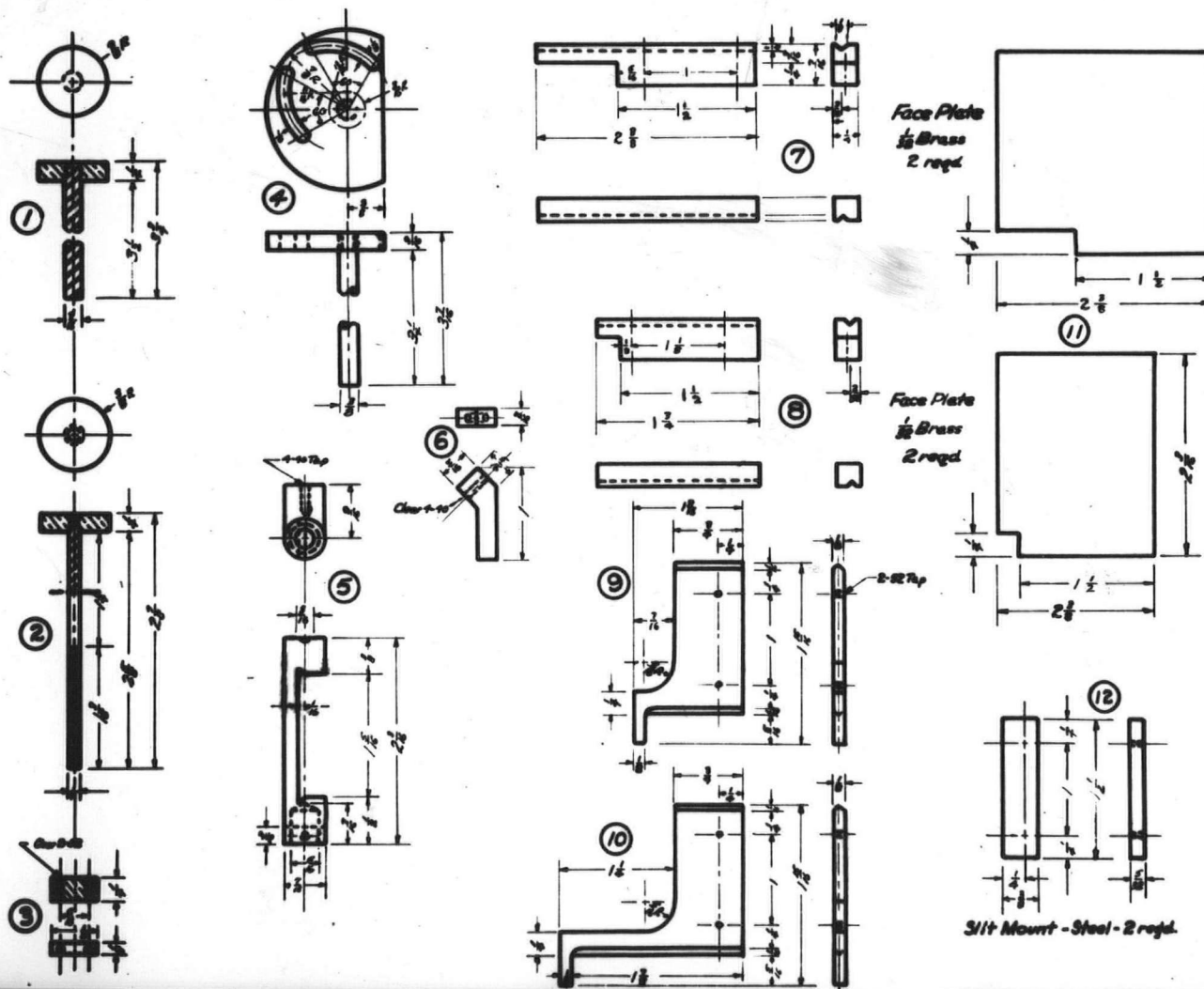


Prism Table
Aluminum, 1 reqd.



Scale:- All Full Size.

PRISM TABLE DETAIL
DRIVE BASE PLATE
MOTOR MOUNT
PHYSICS DEPT., UBC
Drawn By: [Signature]
Date: Jun 8 '50 Sheet No. 5



PARTS LIST

- ① Slit Control - 1 reqd.
 ② Mirror Control - 1 reqd.
 ③ Trunnion - 2 reqd.

No	Name	Qty	Mat
4	Slit Eccentric	1	Br's
5	Mirror Clamp	1	"
6	Clamp Crank	1	Steel
7	Exit Slit Channel	1	Br's
8	Ent. Slit Channel	1	"
9	Ent. Slit Mount	1	Steel
10	Exit Slit Mount	1	Steel

SPECTROGRAPH
 Detail of
 SLITS

Physics Dept - U.B.C.

